JOURNAL OF QUATERNARY SCIENCE (2026) 1–18 ISSN 0267-8179. DOI: 10.1002/jqs.70079

JQS Journal of Quaternary Science QRA Quaternary Research Association

A new, ~4500-year varve record and high-resolution tephrochronology from lake Hämälänlampi, eastern Finland, provides age constraints for the Furnas C and the Glen Garry/Askja A-2000 eruptions

MAARIT KALLIOKOSKI,[1,2]* VEERA EROLA[2] and SAIJA SAARNI[2]
[1]Department of Geosciences and Geography, University of Helsinki, Helsinki, Finland
[2]Department of Geography and Geology, University of Turku, Turku, Finland

Received 17 February 2026; Revised 20 April 2026; Accepted 29 April 2026

ABSTRACT: The northern European distal cryptotephra framework is constantly developing both in terms of identification of new tephra horizons and improved age constraints for the already well-established tephra marker horizons. However, many prehistoric tephra layers have only been dated by the radiocarbon method, with its inherent problems. Here, we present a new ~4500-year, continuously varved lacustrine sediment record and tephrochronology from lake Hämälänlampi, eastern Finland. The varve chronology was established by repeated varve counts from epoxy-impregnated sediment blocks and selected elemental maps (Si, K, Fe and Mn) produced by micro-XRF scanning. The sediment core was investigated for the presence of cryptotephra, and the exact location of the nine identified cryptotephra horizons was pinpointed with either 0.5- or 1-cm depth resolution. The volcanic glass shards were geochemically characterised and correlated to their source eruptions. As a result, we report the first findings of the Hekla 1947, Furnas C and Hekla C tephras in Finnish environmental records, and provide varve ages for the Furnas C, Hekla Y, Hekla C and Öræfajökull 3.5 ka tephras for the first time. We also suggest a new, high-resolution varve age 128–117 BCE for the Glen Garry tephra, based on integration of varve ages from several studies.

KEYWORDS: Finnish tephrochronology; Furnas C tephra; Hekla tephra; Öræfajökull 3.5 ka tephra; varve chronology

Introduction

The northern European Holocene distal cryptotephra framework—an important dating tool of paleoenvironmental records in northern Europe—is constantly developing, and the past couple of decades have witnessed a remarkable increase in research efforts aimed at improving the knowledge on distal cryptotephra occurrences (e.g., Davies et al., 2015; Plunkett and Pilcher, 2018 and references therein) and the eruption histories of the volcanoes that produced them (e.g., Óladóttir et al., 2008, 2011; Johansson et al., 2017; Larsen et al., 2020; Wastegård et al., 2020; Farnsworth et al., 2025). Recent advances in the northern European tephrochronology include identification of new (crypto)tephra horizons, both from European volcanic provinces (Wastegård et al., 2020; Kinder et al., 2020; Kalliokoski et al., 2023) and volcanic regions of other continents (Plunkett and Pilcher, 2018; Jones et al., 2019; Kalliokoski et al., 2023; Carter-Champion et al., 2025), as well as new, improved age constraints for well-known tephra marker horizons through ice-core research (e.g., Mackay et al., 2022; Pearson et al., 2022; Plunkett et al., 2023; Davies et al., 2024) and studies of varved (annually laminated) lake sediment records (e.g., Zillén et al., 2002; Kinder et al., 2020; Walsh et al., 2021, 2023; Carter-Champion et al., 2025).

Precisely dated (crypto)tephra isochrons offer a valuable alternative to the radiocarbon (^{14}C) method for dating environmental records, especially during periods when ^{14}C dating is problematic due to perturbations in the atmospheric radiocarbon content, and consequent plateaus in the ^{14}C curve (Lowe et al., 2001; Guilderson et al., 2005). The power of tephrochronology as a high-precision correlation and dating tool to infer the sequence of response to climatic forcing in various Late Glacial and Holocene environmental archives has already been demonstrated in multiple research projects (e.g., Lind and Wastegård, 2011; Lane et al., 2013; Candy et al., 2025). However, the ages of many prehistoric tephra isochrons in the northern European tephrochronology have thus far been determined by ^{14}C dating the sediments that contain them, which may hinder their utilisation as high-precision dating horizons.

The most precise ages for prehistoric tephra isochrons in Northern Europe are acquired when (crypto)tephra is preserved within ice cores and can be assigned Greenland ice-core ages (GICC05, Vinther et al., 2006; GICC21, Sinnl et al., 2022). The ultra-high precision of tephra ages from Greenland ice cores (GICs) is demonstrated, for example, by new age constraints for the early mid-Holocene Mazama (7562 ± 34 a b1.95k), Mashu i–f (7473 ± 33 a b1.95k) and KS_2 (7089 ± 26 a b1.95k) tephras (Davies et al., 2024), which have age uncertainties of just around 0.9%. At the Mid to Late Holocene transition (around 4.2 ka) and through the Common Era, the uncertainty in age constraints for tephra in the GICs is ~0.4% (e.g., Hekla 4, 4325 ± 8 a b1.95 k in Davies et al., 2024; Mt. Churchill White River Ash, 852 ± 2 CE in Mackay et al., 2022; Torfajökull Landnám-tephra, 877 ± 2 CE in Plunkett et al., 2023). Transferral of these GIC ages to other environmental archives containing the same tephra marker

*Correspondence: M. Kalliokoski, as above.
Email: maarit.kalliokoski@helsinki.fi

horizons enables both the establishment of high-precision tie-points between climate proxy records and an estimation of the accuracy of previously constructed age models (e.g., Candy et al., 2025). Within the northern European tephrochronological framework, this approach is especially well suited to the Alaskan (and other ultra-distal) cryptotephras, with a westerly to northerly main dispersal axis, resulting in cryptotephra fall-out both in Greenland and in northern Europe (e.g., Jensen et al., 2014; van der Bilt et al., 2017, Plunkett and Pilcher, 2018; Davies et al., 2024). However, surprisingly few of the Icelandic silicic tephras that form the core of the northern European distal cryptotephra framework have thus far been identified in the Greenland ice cores (Abbott and Davies, 2012; Plunkett et al., 2023; Davies et al., 2024), which indicates that simultaneous west- and eastward dispersal of Icelandic tephra in detectable amounts may be uncommon.

Another method to refine the ages of the prehistoric tephras is the identification of tephra isochrons in lacustrine sediments that are either continuously varved (Zillén et al., 2002; Kinder et al., 2020) or contain floating varve chronologies that are anchored to calendar years by using additional dating methods (e.g., Dörfler et al., 2012; Walsh et al., 2021). When cryptotephra deposits are embedded in continuously varved lake sediments, their ages can be determined by incremental dating, where the laminae/lamina couplets (i.e., varve years) are counted both from the modern sediment surface downwards (Zillén et al., 2002) and between the prehistoric and historical, or otherwise well-dated tephra horizons (Zillén et al., 2002; Walsh et al., 2021, 2023). Ideally, the accuracy and precision of the obtained tephra ages can be tested by between-site comparison of tephrochronologies from several varved lake sediment records. The most likely age for a tephra can thus be narrowed down as more independent varve chronology-derived tephra ages are published and compared.

Several continuous high-quality varved lacustrine records are known from Finland (e.g., Ojala et al., 2000, 2012; Haltia-Hovi et al., 2007, 2010; Saarni et al., 2015, 2016a, 2016b), the longest of which contain nearly 10 000 varves, such as Korttajärvi, 9590 ± 103 varve years, and Nautajärvi, 9898 ± 97 varve years (Ojala and Tiljander, 2003). The error estimates for even the longest varve chronologies in Finnish lakes are generally within 1–2% of the varve counts (Ojala and Tiljander, 2003; Haltia-Hovi et al., 2011; Saarni et al., 2016a), even though a recent study by Carter-Champion et al. (2025) has revealed that, for example, in Nautajärvi, the varve count errors may be much larger than previously estimated. The varved lake records form the foundation of high-resolution paleoenvironmental studies in Finland, but their potential for tephrochronological studies remains underutilized. Cryptotephra investigations are not routinely conducted on Finnish varved lake records and, thus far, very few cryptotephra horizons have been reported from Finnish varved lakes (Kalliokoski et al., 2019; Carter-Champion et al., 2025). In contrast, the recently published Holocene tephrochronological framework for Finland comprises of 19 geochemically fingerprinted cryptotephra horizons with Icelandic and Alaskan origin (Kalliokoski et al., 2023), which, together with the high number of Finnish lakes containing excellent quality varve records, suggests Finland to be a region of exceptional potential for combining varve chronologies and tephrochronology.

This paper presents a new 4500-year-long varve record and a tephrochronology from a previously unstudied boreal lake Hämälänlampi in central east Finland. Here, the presence of cryptotephra has been utilised in two ways: historical tephras with well-known eruption dates have been used for an independent evaluation of the accuracy of the varve counts and the new varve chronology has been used for providing precise age constraints for the prehistoric Furnas C (Azores) and Glen Garry/Askja 2000 tephras as well as for the first varve ages of the Hekla Y, Hekla C and Öræfajökull 3.5 ka tephras.

Material and methods

Research site

Hämälänlampi is a small (surface area 4.73 ha), but fairly deep (maximum water depth 18.3 m) lake in the municipality of Tohmajärvi in eastern Finland (62.25° N and 30.48° E, 76.6 m.a.s.l.) (Fig. 1). It lies immediately east of a NW-SE-trending esker traversing the zone between the II Salpausselkä and Tuupovaara ice-marginal formations, which were deposited during the Younger Dryas (Rainio, 1982; Lunkka et al., 2020; Fig. 1). There are two inflows into Hämälänlampi, the main one draining water from a larger lake, Pitkälampi, immediately north-west of the Hämälänlampi and another one bringing water from a pond, Pienilampi, into the lake. There is one outlet, Porttipuro, in the southeast corner of the lake draining waters into a larger river, Jänisjoki. The Quaternary deposits that make up most of the catchment area include well-sorted gravels and sands of the esker system that forms a water divide on the western and southern sides of the lake (Fig. 1), and fine-grained cover deposits of mainly coarse silt at lower elevations. The exact timing of first inhabitation on the shores of Hämälänlampi is not known. According to a pollen study from the neighbouring lake Pitkälampi (Fig. 1), rotating slash-and-burn cultivation commenced in the catchment already in the 1450s and remained the main cultivation method until the early 1800s, after which permanent fields replaced the rotational pattern of agriculture (Grönlund and Asikainen, 1992).

Field work

Lake Hämälänlampi was cored during the winter field work seasons in March 2022 and 2023, when the lake ice cover could be used as a coring platform. Four long cores, HÄM-A, HÄM-B, HÄM-C and HÄM-D—covering sediment depths of 0–236 cm, 0–200 cm, 50–280 cm and 115–322 cm, respectively—were recovered from the deepest point of the basin using a rod-operated Livingstone-type piston-corer. To ensure the preservation of the water–sediment interface, a 32-cm-long mini freeze-core (Saarinen and Wenho, 2005) was collected using an HTH gravity-corer (Renberg and Hansson, 2008) and a dry-ice filled aluminium mini-wedge. All the collected cores were stored in the cold room/freezer at the Geology section of the University of Turku (UTU) until laboratory processing commenced.

Sample preparation

Cores HÄM-A (sediment depth 0–236 cm) and HÄM-D (sediment depth 115–322 cm) were cut open lengthwise using a circular saw and a wire, and cores HÄM-B and HÄM-C were archived for later studies. The cleaned surfaces of the core halves were visually logged and photographed for recording their lithologies and correlating the cores. Magnetic susceptibility was measured from the fresh sediment surface of the split cores in 2 mm steps with a Bartington M2 susceptibility metre equipped with an MS2E1 spot reader sensor, and used as an additional aid in core correlation.

The cores were subsampled for geochemical analysis using aluminium moulds (dimensions 11.5 × 2.0 × 1.0 cm). Subsampling was performed with a 1.5 cm overlap between sub-

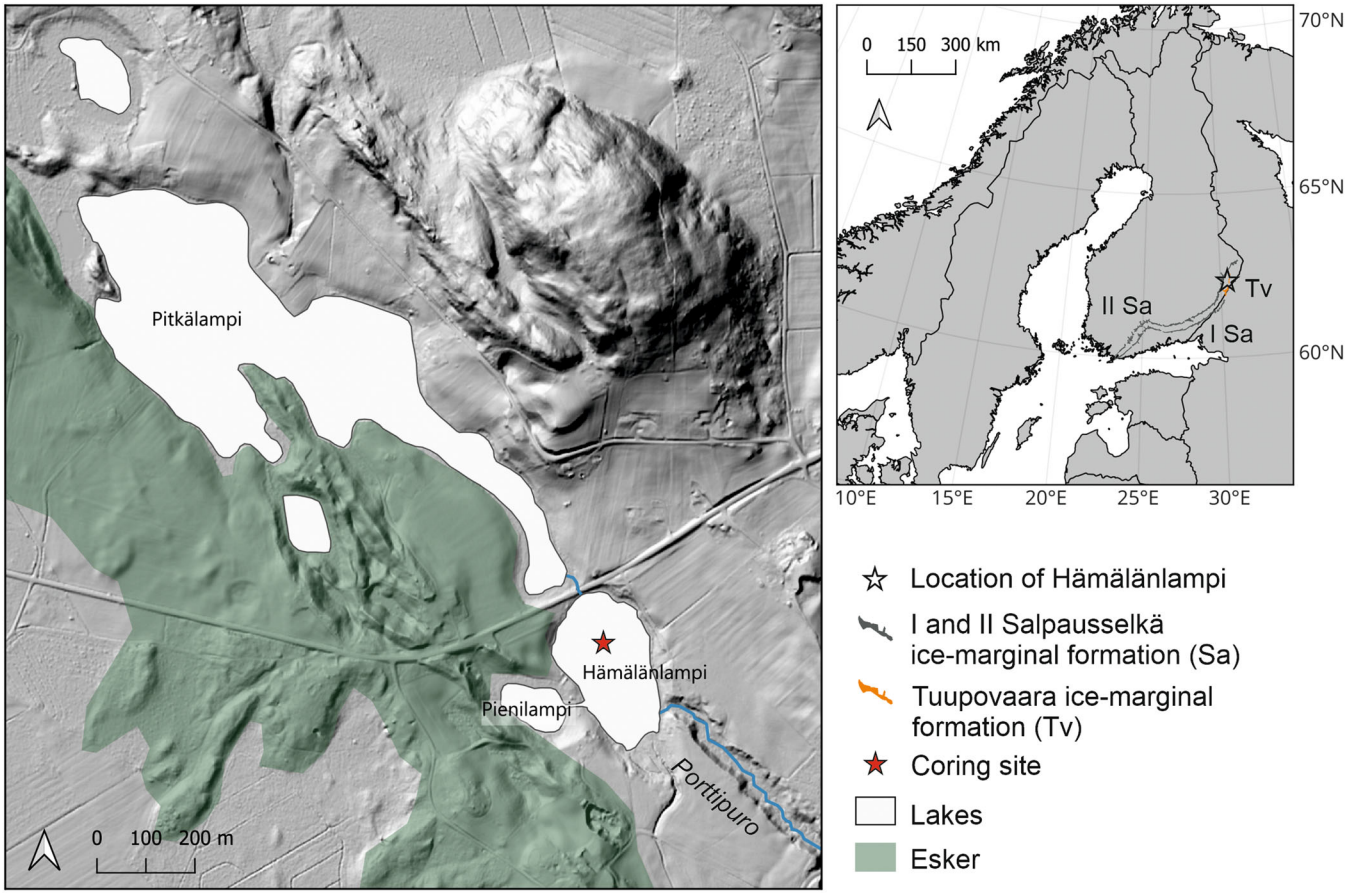

Figure 1. Location of the coring site and catchment topography. The digital elevation model is from the 2 m Hillshade data set produced by the National Land Survey of Finland. The location of Hämälänlampi between the II Salpausselkä (II Sa) and Tuupovaara (TV) ice-marginal formations is marked on the inset map. [Color figure can be viewed at wileyonlinelibrary.com]

sequent samples, and the samples from 0 to 236 cm sediment depth in the HÄM-A core (HÄM-A-1–HÄM-A-23) were impregnated with Spurr epoxy according to the water–acetone–epoxy exchange method first described in Lamoureux (1994). The subsamples from 130–322 cm depth in the HÄM-D core (HÄM-D-1–HÄM-D-19) were impregnated in Araldite epoxy using a modified shock–freeze and freeze–dry method (Lotter and Lemcke, 1999; Salminen et al., 2021). Two 10-cm-long thin sections for microfacies analysis were prepared from the cured sediment blocks HÄM-A-6 and HÄM-A-12 at the thin-section facility of UTU following the procedure described in Lotter and Lemcke (1999). The sediment blocks for thin-section preparation were selected to provide information on varve structure at sediment depths with both thick (HÄM-A-6) and thin (HÄM-A-12) varves. All the sediment blocks were photographed under a stereomicroscope after polishing, and the thin sections were photographed under a petrographic microscope.

Micro-XRF scanning

X-ray fluorescence (XRF) spectrometry is routinely used in lake sediment studies for producing information on downcore element variations in lacustrine sediments (e.g., Rothwell and Croudace, 2015; Croudace et al., 2019 and references therein). The downcore element variation in Hämälänlampi sediment was measured from polished sample surfaces of HÄM-A and HÄM-D epoxy blocks with a Bruker Tornado M4 energy-dispersive μ-XRF (rhodium X-ray tube, anode current 500 μA, voltage 50 kV and spot size 20 μm) at UTU. High-resolution elemental maps were produced using 20 μm scanning steps and a 15 ms/pixel counting time.

The semiquantitative elemental composition of sediments and selected element ratios, obtained by μ-XRF scanning, have been used as proxies for, for example, the detrital minerogenic input reflecting seasonal flood events (Si, Ti, K and Al; Martin-Puertas et al., 2010; Czymzik et al., 2010; Saarni et al., 2016b), changes in the lake mixing regime (Fe, Mn and their ratio; Żarczyński et al., 2019; Lincoln et al., 2025), carbonate precipitation (Martin-Puertas et al., 2010; Bonk et al., 2016) and human-induced environmental changes (Billah et al., 2026). The seasonal change in sediment availability and composition is reflected in elemental maps, which reveal the alternating seasonal lamina couplets. Here, the elemental maps (Si, K, Fe and Mn) are used simultaneously to facilitate reliable identification of varve boundaries and improved precision of varve counting.

Microfacies analysis and varve counting

The structure of the varves was investigated from thin sections under a microscope to understand the annual cycle of deposition. Varves were counted using elemental maps of Si, K, Fe and Mn, as well as microscope photographs of epoxy blocks and thin sections to ensure the robustness of the constructed varve chronology. The varve counts were performed in c. 10-cm-long sequences, where 34 marker varves (varves with distinct appearance, e.g., exceptional thickness) served as boundaries. Independent error estimates for each marker varve-constrained varve sequence were obtained by counting the varves three times (Lotter and Lemcke, 1999), and error estimates for the whole chronology were calculated from these. Individual lamina thicknesses were not measured, but

average varve thicknesses were calculated from varve counts for each 1-cm sediment interval.

Tephra work

First, 2-cm-long contiguous subsamples were taken from cores HÄM-A and HÄM-D for an initial cryptotephra screening. The samples were dried at 105 °C overnight, weighed, combusted at 550 °C for 4 h and treated with 10% HCl to remove organic matter and carbonates. The loss-on-ignition values for the sediment were calculated after the combustion (e.g., Heiri et al., 2001). The samples were then sieved using 90 μm and 25 μm meshes, and volcanic glass was concentrated using the heavy liquid separation method described in Turney, 1998. For this step, 2.3 and 2.6 g/cm^3 densities of LST Fastfloat heavy liquid were used in accordance with the typical density range of Icelandic rhyolitic to andesitic cryptotephra (Kalliokoski et al., 2020). The samples were mounted on glass slides using Canada Balsam, and where volcanic glass shards were identified under a polarising microscope, a new set of subsamples was prepared for narrowing down the exact depth of maximum shard concentration. Subsampling resolution was guided by the varve thickness; a resolution of 1 cm (0.5 cm) was used for sections with thick (thin) varves.

New samples were taken from the depth of peak shard concentration for characterising the geochemical composition of the volcanic glass with an electron microprobe. Instead of combustion, the organic matter was removed using the acid digestion method (Pilcher and Hall,1992; Dugmore et al., 1995). Otherwise, the sample preparation followed the same procedure as that during the initial screening. Since all the cryptotephra deposits in lake Hämälänlampi contain very few shards, a micromanipulator was used for individually picking the shards (see Lane et al., 2014; MacLeod et al., 2014). The shards were mounted in epoxy, and the samples were sanded and polished to 10–25 μm thickness and carbon-coated at the Institute of Earth Sciences (IES), University of Iceland (UI). Electron probe microanalyses (EPMA) of major elements were conducted using a JEOL JXA-8230 SuperProbe at the IES, UI (see Supplementary material S1 for a description of the analysis procedure, secondary standards and microprobe configuration).

Results and interpretation

Sediment properties

The investigated cores are laminated throughout, and no homogenic sequences were observed. No attempt was made to core the deeper sediments, and the full extent of the varved sequence in Hämälänlampi remains unknown. The lowermost sediment (258–322 cm) in the HÄM-D core shows disturbance structures (Fig. 2(B)), which are most likely related to coring and gas expansion.

Microfacies analysis of the Hämälänlampi sediment from thin sections reveals clastic–biogenic annual couplets of laminae, the most common type of varves encountered in Finnish lakes (Ojala et al., 2000). The varve structure comprises of a minerogenic lamina deposited during snow-melt-induced spring flooding, followed by a biogenic lamina representing accumulation during the growing season (Fig. 2(C), see, e.g., Saarni et al., 2017; Salminen et al., 2023). The average varve thickness is around 0.5 mm and a distinct increase in varve thickness is noted at around 111 cm depth (Fig. 2(A)). This development coincides broadly with decreasing sediment organic content from initial LOI ~50% to ~20% towards the top of the core. The varve thickness above the 111 cm depth varies generally between 1 and 5 mm, but reaches c. 10 mm in the uppermost 15 cm due to a high water content and the uncompacted nature of the surface sediment. Thus, the uppermost 15 cm are excluded from the description of the varve characteristics (Fig. 2(A)).

Varve chronology

The new varve record from Hämälänlampi contains 4543 (−87/+30) varves (age–depth plot in Supplementary material S1). Varve counts and error estimates for each counted interval and the whole core are presented in Table 1, and varve counts between geochemically fingerprinted tephra deposits are available in Supplementary material S1. Varve counts from thin sections and epoxy blocks show similar results, and the varve quality is generally good. The cumulative varve count uncertainty is <2.0% at 0–263 cm sediment depth and 2.6% for the full varve chronology. There are two sections of poorer varve quality at depths of 253–273 cm and 293–312 cm, corresponding to calendar ages 1802–1383 (−55/+28) BCE and 2384–2095 (−83/+28) BCE, respectively (Fig. 2(B); Table 1).

Tephrochronology

Tephra screening indicated the presence of 10 cryptotephra deposits in Lake Hämälänlampi at 31–33 cm, 55–57 cm, 115–116 cm, 132–133 cm, 169–171 cm, 187–187.5 cm, 193.5–194 cm, 210–210.5 cm, 219.5–220 cm and 257.5–258 cm sediment depth (Fig. 2(A)). All the cryptotephra horizons are well confined, which indicates the deposits to consist mainly of primary fall-out. No post-depositional migration or background deposition of tephra shards was detected and, thus, a rapid and efficient delivery of shards from the catchment into the sediment can be assumed. Shard concentration in all the deposits is low, mostly <30 shards/g of dry sediment (Fig. 2(A)). This, together with the small shard size and common presence of vesicles in the volcanic glass (Fig. 2(D)), resulted in a low number of successful EPMA results for three of the deposits (Table 2). No EPMA results were obtained from the minor amount of tephra at 169–171 cm depth. Only results with analytical totals >95% are included in establishing tephra correlations, as recommended by Hunt and Hill (1993), but all analysis results are published in Supplementary material S1.

Geochemical compositions of the cryptotephra deposits in Hämälänlampi were compared against geochemistry of both proximal (Johansson et al., 2017; Wastegård et al., 2020) and distal (e.g., Chambers et al., 2004; Kinder et al., 2020) products of the Azorean volcanoes, and extensive proximal and distal data sets for several Icelandic volcanoes (e.g., Larsen et al., 1999; Guðmundsdóttir et al., 2011; Óladóttir et al., 2011; Plunkett and Pilcher, 2018; Meara et al., 2020; Kalliokoski et al., 2020, 2023). However, only the most likely correlates according to geochemical composition and assumed age are shown in the bivariate plots of major element ratios for the sake of clarity (Fig. 4(A)–(D)).

Hekla 1947 (Häm 31–33 cm)

The cryptotephra deposit at 31–33 cm sediment depth consists of scarce, brown shards with vesicular and fluted morphologies (a in Fig. 2(A), (B), (D)). Geochemical results were obtained only from one tephra glass grain due to the low number of shards (13 shards/g of dry sediment) in this horizon (Table 2; Fig. 3). Plotting of the EPMA results on the total alkali–silica (TAS) diagram indicates a dacitic, low-alkali

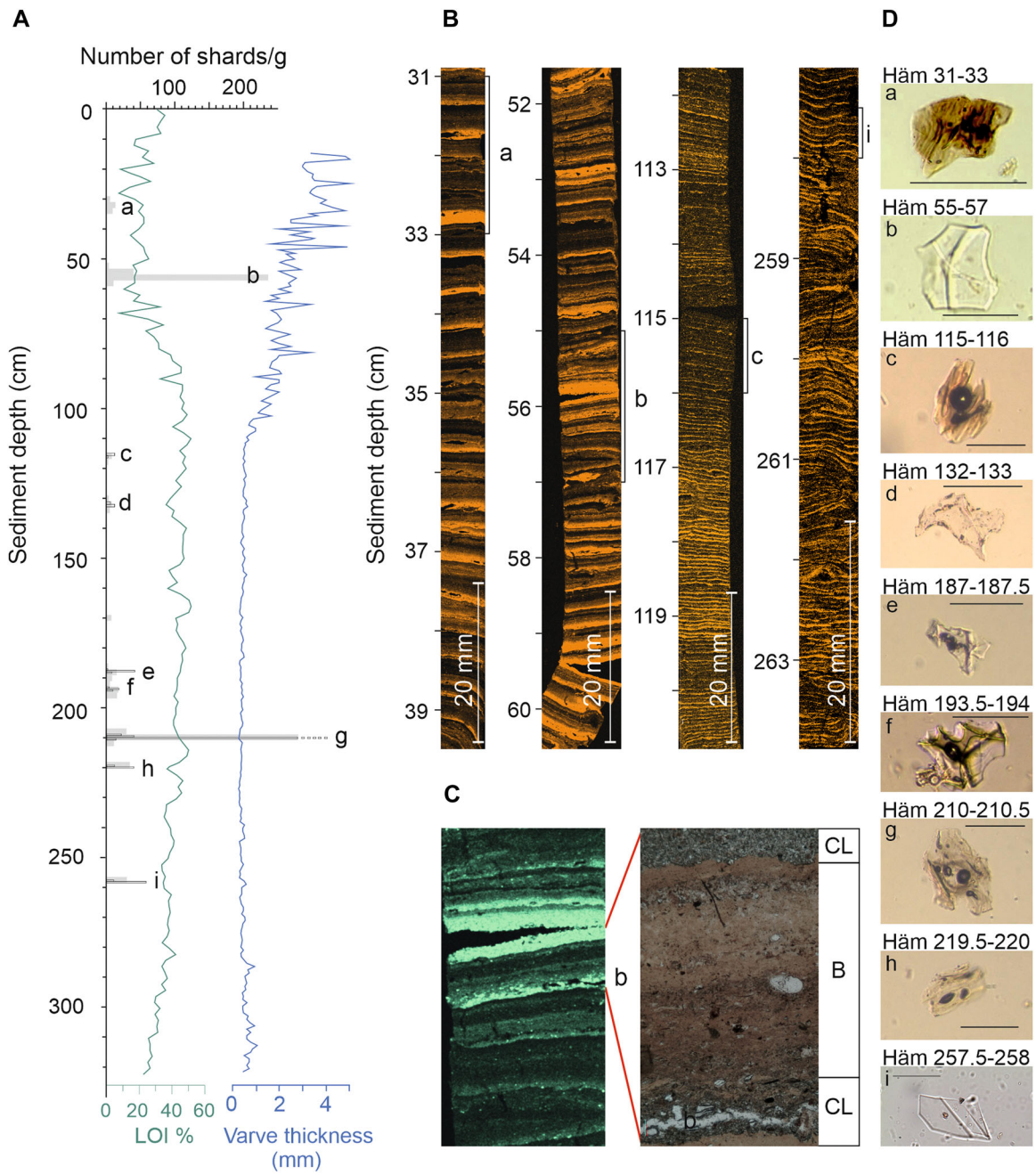

Figure 2. (A) Loss on ignition and average varve thickness, together with volcanic glass shard concentrations of the cryptotephra deposits (labelled a–i) in Hämäläänlampi. (B) Occurrence depths of selected cryptotephra deposits marked on micro-XRF elemental maps of K. The downcore decrease in varve thickness demands higher-resolution sampling for precise age determination of pre-historic tephras. The disturbed sediment sections below c. 258 cm depth are clearly visible in the elemental map. (C) Elemental map of Si from the occurrence depth of the tephra layer b and a photograph of a thin section demonstrating the clastic–biogenic varve structure in Hämäläänlampi. B, biogenic lamina; CL, clastic lamina. A couple of volcanic glass shards are visible in the lower clastic lamina. (D) Microscope images of the nine cryptotephra deposits a–i. The scalebar length is 40 µm. [Color figure can be viewed at wileyonlinelibrary.com]

composition and an origin in the Icelandic Hekla volcano for this deposit (Fig. 3).

This cryptotephra can be tentatively correlated to the Hekla 1947 eruption by comparing the geochemical composition (Fig. 4(B)) with volcanic glass from other historical Hekla eruptions and the Hekla 1947 tephra samples that were collected from a visible fall-out in Finland in 1947 (Salmi, 1948, Kalliokoski et al., 2020). A higher number of successful EPMA results are generally needed for confidently assigning a cryptotephra to its source eruption. However, this cryptotephra deposit is well confined in Hämäläänlampi sediment record above the Askja 1875 tephra, and no background input of cryptotephra shards is observed, which indicates this deposit to represent primary fall-out. The varve age (1946–1951 CE) of this deposit in Hämäläänlampi, together with historical observations of the Hekla 1947 tephra dispersal to Finland, is considered convincing evidence of its origin. Thus, we suggest this deposit to represent the first geochemically confirmed finding of the Hekla 1947 tephra in Finnish environmental records.

Askja 1875 (Häm 55–57 cm)

This cryptotephra horizon has a relatively high shard concentration for a distal site in Finland (235 shards/g of dry sediment), and a couple of shards are even visible in a thin section, which enables pinpointing of the location of this cryptotephra to a single varve (Fig. 2(C)). The shards are

Table 1. Varve counts and varve count uncertainties of the Hämälänlampi core shown for each marker varve-constrained interval and for the full core length.

Marker varve interval	Depth in the core (cm)	Nr. of varves	Nr. of varves cumul.	Calendar years (CE/BCE)	Difference between 3 counts (−/+)	Cumulative difference (−/+)	Error %	Error % cumul.
0–1	0.0–16.2	30	30	1991–2021 CE	0/0	0/0	0.0	0.0
1–2	16.2–20.0	11	41	1980–1991 CE	0/0	0/0	0.0	0.0
2–3	20.0–25.0	12	53	1968–1980 CE	0/0	0/0	0.0	0.0
3–4	25.0–30.5	15	68	1953–1968 CE	0/0	0/0	0.0	0.0
4–5	30.5–41.0	30	98	1923–1953 CE	0/0	0/0	0.0	0.0
5–6	41.0–51.2	33	131	1890–1923 CE	0/0	0/0	0.0	0.0
6–7	51.2–61.1	39	170	1851–1890 CE	1/0	1/0	2.5	0.6
7–8	61.1–70.2	40	210	1811–1851 CE	0/0	1/0	0.0	0.5
8–9	70.2–80.2	50	260	1761–1811 CE	0/3	1/3	6.4	1.5
9–10	80.2–90.4	49	309	1712–1761 CE	1/0	2/3	2.0	1.6
10–11	90.4–100.5	59	368	1653–1712 CE	2/0	4/3	3.4	1.9
11–12	100.5–111.0	95	463	1558–1653 CE	2/0	6/3	2.1	1.9
12–13	111.0–120.9	159	622	1399–1558 CE	3/0	9/3	1.9	1.9
13–14	120.9–130.7	197	819	1202–1399 CE	1/0	10/3	0.5	1.6
14–15	130.7–140.6	189	1008	1013–1202 CE	0/5	10/8	2.7	1.8
15–16	140.6–150.5	219	1227	794–1013 CE	4/2	14/10	2.7	2.0
16–17	150.5–160.4	197	1424	597–794 CE	0/0	14/10	0.0	1.7
17–18	160.4–171.0	208	1632	389–597 CE	2/2	16/12	1.9	1.7
18–19	171.0–177.3	210	1842	179–389 CE	4/0	20/12	1.9	1.7
19–20	177.3–182.3	95	1937	84–179 CE	0/0	20/12	0.0	1.7
20–21	182.3–193.8	227	2164	144 BCE–84 CE	2/0	22/12	1.5	1.6
21–22	193.8–203.8	189	2353	333–144 BCE	0/0	22/12	0.0	1.4
22–23	203.8–214.0	238	2591	571–333 BCE	1/0	23/12	0.4	1.4
23–24	214.0–223.7	237	2828	808–571 BCE	1/0	24/12	0.4	1.3
24–25	223.7–233.8	240	3068	1048–808 BCE	0/1	24/13	0.4	1.2
25–26	233.8–243.5	142	3210	1190–1048 BCE	4/0	28/13	2.8	1.3
26–27	243.5–253.3	193	3403	1382–1190 BCE	2/0	30/13	1.0	1.3
27–28	253.3–263.0	248	3651	1631–1383 BCE	10/10	40/23	8.1	1.7
28–29	263.0–272.9	171	3822	1802–1631 BCE	15/5	55/28	11.7	2.2
29–30	272.9–282.9	201	4023	2003–1802 BCE	6/0	61/28	3.0	2.2
30–31	282.9–292.4	92	4115	2095–2003 BCE	0/0	61/28	0.0	2.2
31–32	292.4–302.1	172	4287	2267–2095 BCE	13/0	74/28	7.6	2.4
32–33	302.1–311.7	117	4404	2384–2267 BCE	9/0	83/28	7.7	2.5
33–34	311.7–321.6	139	4543	2523–2384 BCE	4/2	87/30	4.3	2.6
Total	0–321.6 cm	4543	4543	2523 BCE–2021 CE	87/30	87/30		2.6

colourless and of mixed morphologies, including vesicular, cuspate, fluted and platy shards (b in Fig. 2(D)). EPMA results from 19 volcanic glass shards reveal a rhyolitic composition (Fig. 3) and relatively high TiO_2 and FeO_{tot} contents (Table 2), typical for the volcanic glass of the Icelandic Askja central volcano.

The correlation of this Askja cryptotephra deposit to an eruption in 1875 can be made based on its highly silicic nature (SiO_2 72.06–73.95 wt %) and diagnostic, high TiO_2 content (0.74–0.89 wt %; Fig. 4(C)), as demonstrated by Larsen et al. (1999). In addition to the rhyolitic glass, a dacitic component of the Askja 1875 has also been encountered in Finland (Kalliokoski et al., 2019), Sweden (Boygle, 2004; Borgmark and Wastegård, 2008) and Poland (Kinder et al., 2020) but is absent from the Hämälänlampi record.

The Askja 1875 tephra forms one of the most important tephra isochrons in Fennoscandia, due to its wide dispersal, high shard concentrations and potential to provide precise age constraint for the growing anthropogenic influence of the past 200 years in Finland (Kalliokoski et al., 2019). This isochron also provides a means to test the accuracy of varve counts and to verify the annual nature of laminations in varved lacustrine sediments, thereby lending support for tying the uncompacted surface sediment section to calendar years. In Hämälänlampi, the varve chronological age of the Askja 1875 cryptotephra is 1871–1878 CE, and the deposit can be constrained to a single varve (varve 1875 CE according to varve counts) based on inspection of thin sections (Fig. 2(B), (C)).

Hekla 1510 (Häm 115–116 cm)

The cryptotephra deposit at 115–116 cm sediment depth contains brown volcanic glass shards with vesicular and fluted morphologies (c in Fig. 2(D)). This deposit contains a very low concentration of volcanic glass grains (8 shards/g of dry sediment), and the geochemical composition of the three successfully analysed shards falls within the envelope of Hekla central volcano on the TAS diagram (Fig. 3).

This cryptotephra could be correlated either to the Hekla 1510 or the Hekla 1947 eruption based on its geochemical composition (Fig. 4(B)). Among the historical Hekla tephras, Hekla 1947 and Hekla 1510 have identical major element geochemistry (Larsen et al., 1999), but their age difference is sufficient for distinguishing between the two on stratigraphic grounds. The stratigraphic position of this deposit below the Askja 1875 tephra in Hämälänlampi indicates an origin in the Hekla 1510 eruption. This correlation is further supported by earlier identifications of the Hekla 1510 cryptotephra in Finnish environmental records (Kalliokoski et al., 2020, 2023) and the varve age (1500–1516 (−9/+3) CE) of this deposit in Hämälänlampi.

Table 2. Normalised major element compositions of volcanic glass shards from Lake Hämälänlampi.

Sample name and correlation	SiO_2	TiO_2	Al_2O_3	FeO	MnO	MgO	CaO	Na_2O	K_2O	P_2O_5	Total
Häm 31–33 Hekla 1947	63.69	0.87	15.31	7.83	0.22	1.22	4.58	4.17	1.76	0.33	100
Häm 55–57 Askja 1875	73.95	0.77	13.36	3.34	0.12	0.68	2.20	2.91	2.44	0.23	100
	73.76	0.77	12.91	2.97	0.08	0.77	2.54	3.73	2.37	0.10	100
	73.67	0.84	12.50	3.48	0.11	0.74	2.59	3.57	2.28	0.22	100
	73.50	0.82	12.89	3.26	0.10	0.72	2.41	3.79	2.31	0.20	100
	73.47	0.89	12.63	3.38	0.14	0.64	2.65	3.79	2.35	0.07	100
	73.44	0.83	12.70	3.36	0.12	0.69	2.53	3.70	2.42	0.20	100
	73.44	0.77	12.86	3.30	0.07	0.69	2.44	3.88	2.35	0.19	100
	73.39	0.78	12.76	3.69	0.14	0.74	2.60	3.39	2.35	0.17	100
	73.35	0.79	12.76	3.41	0.15	0.71	2.62	3.67	2.40	0.14	100
	73.31	0.85	12.76	3.49	0.09	0.76	2.50	3.80	2.26	0.17	100
	73.30	0.81	12.84	3.35	0.12	0.68	2.35	3.99	2.37	0.19	100
	73.26	0.74	13.00	3.53	0.14	0.75	2.63	3.44	2.34	0.19	100
	73.24	0.87	12.79	3.73	0.15	0.80	2.59	3.22	2.45	0.16	100
	73.21	0.80	12.75	3.54	0.09	0.77	2.59	3.59	2.41	0.24	100
	73.19	0.82	12.95	3.64	0.11	0.71	2.69	3.29	2.48	0.13	100
	73.17	0.81	13.09	3.59	0.12	0.83	2.62	3.41	2.17	0.18	100
	72.98	0.85	12.80	3.75	0.15	0.76	2.77	3.44	2.34	0.16	100
	72.90	0.83	12.95	3.61	0.10	0.77	2.50	3.95	2.28	0.11	100
	72.06	0.88	13.00	4.01	0.13	0.82	2.79	3.79	2.35	0.16	100
Mean ($n = 19$)	73.29	0.82	12.86	3.50	0.12	0.74	2.56	3.60	2.35	0.17	100
SD	0.39	0.04	0.19	0.23	0.02	0.05	0.14	0.28	0.07	0.04	0
Häm 115–116 Hekla 1510	66.99	1.29	14.10	5.84	0.19	1.17	3.16	4.15	2.77	0.35	100
	62.85	0.86	15.68	8.07	0.22	1.40	4.62	4.29	1.68	0.34	100
	62.86	0.90	15.65	7.86	0.25	1.47	4.45	4.61	1.65	0.30	100
Häm 132–133 Hekla 1158	68.16	0.43	15.03	5.36	0.21	0.47	3.12	4.88	2.30	0.03	100
	68.56	0.44	15.39	5.47	0.20	0.39	3.08	4.25	2.18	0.04	100
Mean ($n = 2$)	68.36	0.43	15.21	5.42	0.20	0.43	3.10	4.57	2.24	0.04	100
Häm 187–187.5 Furnas C	64.61	0.40	17.92	3.55	0.27	0.27	0.75	6.86	5.32	0.05	100
	64.31	0.44	17.82	3.45	0.27	0.28	0.83	7.04	5.50	0.07	100
	64.30	0.40	17.70	3.48	0.28	0.25	0.74	7.27	5.55	0.04	100
	64.37	0.32	17.82	3.52	0.27	0.25	0.84	7.06	5.53	0.01	100
	63.91	0.37	17.68	3.59	0.29	0.30	0.77	7.45	5.60	0.05	100
	64.22	0.41	17.96	3.52	0.29	0.28	0.85	6.62	5.78	0.07	100
	63.82	0.38	17.70	3.53	0.26	0.28	0.75	7.71	5.49	0.08	100
	63.87	0.37	17.83	3.53	0.31	0.27	0.77	7.48	5.52	0.06	100
	63.71	0.41	17.71	3.71	0.30	0.24	0.77	7.44	5.64	0.06	100
	64.63	0.27	18.40	2.85	0.23	0.20	0.84	7.11	5.41	0.06	100
	64.55	0.42	17.88	3.63	0.31	0.31	0.77	6.58	5.49	0.06	100
	64.20	0.44	17.64	3.54	0.25	0.30	0.67	7.51	5.43	0.02	100
	64.06	0.37	17.98	3.63	0.30	0.29	0.79	6.91	5.59	0.08	100
	64.06	0.38	18.04	3.49	0.29	0.29	0.78	7.35	5.32	0.00	100
	63.99	0.39	17.60	3.49	0.30	0.29	0.74	7.63	5.49	0.08	100
	63.94	0.32	17.79	3.59	0.28	0.25	0.78	7.46	5.57	0.02	100
	63.93	0.40	17.59	3.64	0.26	0.29	0.74	7.83	5.31	0.02	100
	63.85	0.41	17.73	3.66	0.32	0.28	0.73	7.61	5.40	0.02	100
	63.85	0.39	17.79	3.50	0.26	0.27	0.86	7.51	5.57	0.02	100
	63.83	0.40	17.68	3.65	0.26	0.27	0.74	7.71	5.41	0.04	100
Mean ($n = 20$)	64.10	0.38	17.81	3.53	0.28	0.27	0.77	7.31	5.50	0.05	100
SD	0.28	0.04	0.19	0.18	0.02	0.03	0.05	0.36	0.12	0.02	0
Häm 193.5–194 Glen Garry/Askja ~2000	74.41	0.49	13.06	3.64	0.13	0.40	2.23	3.56	1.99	0.09	100
	73.98	0.54	12.94	3.76	0.10	0.40	2.39	3.80	2.01	0.09	100
	73.92	0.54	13.02	3.73	0.09	0.39	2.37	3.89	2.01	0.04	100
	73.74	0.54	12.98	3.71	0.11	0.43	2.40	4.03	1.99	0.07	100
	73.90	0.45	12.93	3.72	0.10	0.42	2.51	3.77	2.11	0.09	100
	74.62	0.49	13.13	3.59	0.13	0.37	2.44	3.20	1.96	0.07	100
	72.25	0.69	13.61	4.48	0.17	0.59	2.89	3.38	1.80	0.13	100
	71.86	0.69	13.11	4.60	0.13	0.61	2.95	4.01	1.87	0.16	100
	68.65	0.93	13.62	5.83	0.16	1.02	3.87	3.99	1.70	0.23	100
	74.59	0.51	12.88	3.62	0.09	0.45	2.12	3.73	1.89	0.12	100
	74.47	0.43	13.25	3.44	0.08	0.38	2.16	3.78	1.96	0.05	100
	74.19	0.55	12.84	3.74	0.09	0.38	2.37	3.78	1.99	0.08	100
	74.04	0.50	13.26	3.67	0.05	0.45	2.21	3.72	1.97	0.14	100
	74.03	0.46	13.17	3.48	0.08	0.44	2.14	4.29	1.84	0.08	100
	74.02	0.50	12.84	3.64	0.09	0.40	2.23	4.35	1.90	0.03	100
	73.93	0.46	12.97	3.69	0.09	0.46	2.27	4.14	1.91	0.09	100
	73.85	0.49	12.96	3.69	0.09	0.43	2.33	4.14	1.97	0.06	100
	73.83	0.48	12.85	3.69	0.11	0.38	2.20	4.39	2.01	0.06	100
	73.74	0.48	13.10	3.56	0.09	0.39	2.37	4.24	1.91	0.12	100
	73.61	0.51	12.85	3.80	0.11	0.40	2.36	4.20	2.02	0.12	100

(*Continued*)

Table 2. (*Continued*)

Sample name and correlation	SiO_2	TiO_2	Al_2O_3	FeO	MnO	MgO	CaO	Na_2O	K_2O	P_2O_5	Total
	72.62	0.71	13.20	4.24	0.12	0.55	2.65	3.86	1.95	0.10	100
	72.15	0.60	13.38	4.41	0.09	0.54	2.84	4.14	1.73	0.11	100
	72.08	0.62	13.61	4.43	0.12	0.56	2.71	3.80	1.92	0.16	100
	71.89	0.64	13.18	4.31	0.10	0.61	2.82	4.39	1.85	0.20	100
	71.82	0.62	13.39	4.46	0.10	0.64	2.84	4.09	1.87	0.16	100
Mean ($n = 25$)	73.29	0.56	13.13	3.96	0.11	0.48	2.51	3.95	1.92	0.11	100
SD	1.34	0.11	0.24	0.53	0.03	0.14	0.38	0.30	0.09	0.05	0
Häm 210–210.5 Hekla Y	64.87	0.88	15.96	6.35	0.14	1.35	4.72	3.93	1.52	0.29	100
	64.80	0.85	15.77	6.67	0.14	1.32	4.47	4.08	1.56	0.34	100
	64.16	0.97	15.92	6.68	0.17	1.44	4.76	4.00	1.49	0.42	100
	65.02	0.90	15.63	6.50	0.18	1.35	4.76	3.85	1.50	0.32	100
	65.05	0.91	15.54	6.79	0.18	1.30	4.45	3.84	1.66	0.28	100
	64.54	0.94	15.96	6.64	0.14	1.40	4.72	3.93	1.45	0.29	100
	64.89	0.89	15.68	6.60	0.19	1.34	4.50	4.10	1.55	0.27	100
	64.63	0.97	15.69	6.79	0.16	1.43	4.75	3.75	1.53	0.32	100
	64.64	0.97	15.37	6.95	0.20	1.28	4.50	4.05	1.67	0.36	100
	64.01	0.99	15.47	7.13	0.19	1.41	4.62	4.14	1.69	0.34	100
	65.48	0.91	15.81	6.30	0.16	1.27	4.57	3.59	1.53	0.39	100
	64.73	0.90	15.83	6.40	0.14	1.42	4.55	4.25	1.50	0.29	100
	64.32	0.97	15.80	6.63	0.21	1.42	4.48	4.17	1.60	0.41	100
	64.37	0.88	15.68	6.57	0.17	1.50	4.74	4.31	1.47	0.31	100
	63.62	0.99	15.67	7.22	0.23	1.53	4.88	3.89	1.55	0.43	100
	63.89	0.86	15.64	6.74	0.19	1.45	4.85	4.54	1.55	0.29	100
	63.73	0.92	16.05	6.92	0.13	1.40	4.62	4.36	1.54	0.33	100
	63.85	0.99	15.86	6.79	0.15	1.40	4.67	4.37	1.52	0.39	100
	64.23	0.91	15.62	6.69	0.19	1.45	4.71	4.20	1.58	0.42	100
	64.30	0.88	15.65	6.72	0.18	1.41	4.82	4.15	1.48	0.41	100
	63.86	1.04	15.78	6.84	0.16	1.47	4.73	4.22	1.51	0.40	100
	64.00	0.91	15.64	6.95	0.21	1.44	4.82	4.16	1.58	0.29	100
	64.07	0.97	15.78	6.59	0.13	1.40	4.79	4.33	1.62	0.33	100
	63.35	0.89	15.99	6.97	0.16	1.51	4.84	4.42	1.46	0.41	100
	63.73	0.94	15.80	6.90	0.16	1.50	4.69	4.26	1.55	0.47	100
	63.36	0.98	15.62	7.11	0.21	1.51	4.95	4.28	1.60	0.39	100
	63.73	1.00	15.71	7.16	0.16	1.54	4.88	3.95	1.49	0.37	100
	64.17	0.99	16.12	6.66	0.18	1.42	4.69	3.86	1.57	0.35	100
	63.27	1.03	15.67	7.29	0.20	1.56	4.87	4.12	1.55	0.44	100
	63.98	1.00	15.91	6.85	0.21	1.44	4.91	3.82	1.54	0.34	100
	63.84	1.03	15.81	6.95	0.17	1.42	4.88	4.05	1.49	0.37	100
	64.60	0.91	15.83	6.83	0.13	1.40	4.58	3.79	1.61	0.32	100
	63.68	0.97	16.06	6.80	0.18	1.55	4.78	4.06	1.46	0.45	100
	60.55	1.22	15.96	8.32	0.20	1.91	5.60	4.33	1.40	0.51	100
Mean ($n = 34$)	64.10	0.95	15.77	6.83	0.17	1.44	4.74	4.09	1.54	0.36	100
SD	0.82	0.07	0.17	0.35	0.03	0.11	0.21	0.22	0.07	0.06	0
Häm 219.5–220 Hekla C	65.27	0.87	16.20	6.17	0.15	1.15	4.57	3.86	1.50	0.26	100
	65.54	0.86	15.83	6.20	0.16	1.20	4.17	3.99	1.74	0.31	100
	65.35	0.79	16.12	6.44	0.18	1.26	4.41	3.58	1.55	0.31	100
	64.74	0.81	15.81	6.34	0.17	1.25	4.61	4.36	1.61	0.30	100
	65.22	0.84	16.00	6.15	0.15	1.35	4.34	4.12	1.51	0.31	100
	64.85	0.78	15.95	6.43	0.18	1.32	4.68	3.99	1.51	0.29	100
	65.19	0.84	15.65	6.42	0.19	1.35	4.49	4.01	1.60	0.27	100
Mean ($n = 7$)	65.17	0.83	15.94	6.31	0.17	1.27	4.47	3.99	1.58	0.29	100
SD	0.28	0.03	0.19	0.13	0.02	0.08	0.18	0.24	0.08	0.02	0
Häm 257.5–258 Ö-3.5 ka	72.95	0.22	13.25	3.38	0.10	0.01	0.88	5.43	3.78	0.00	100
	73.30	0.22	13.41	3.28	0.11	0.03	0.95	4.93	3.75	0.03	100
	73.28	0.23	13.39	3.30	0.14	0.03	0.89	4.97	3.79	0.00	100
	73.16	0.27	13.44	3.34	0.12	0.02	0.93	5.00	3.72	0.01	100
	73.37	0.20	13.36	3.31	0.12	0.02	0.83	4.77	4.00	0.02	100
	73.16	0.24	13.29	3.28	0.13	0.03	0.91	5.07	3.89	0.00	100
	73.01	0.27	13.35	3.35	0.11	0.02	0.94	5.35	3.59	0.01	100
	73.32	0.21	13.27	3.28	0.12	0.03	0.90	5.09	3.77	0.00	100
	73.58	0.24	13.48	3.33	0.11	0.00	0.86	4.61	3.76	0.02	100
	73.24	0.26	13.39	3.38	0.13	0.01	0.93	4.93	3.71	0.01	100
	73.05	0.18	13.57	3.26	0.09	0.00	0.93	4.97	3.93	0.00	100
Mean ($n = 11$)	73.22	0.23	13.38	3.32	0.12	0.02	0.90	5.01	3.79	0.01	100
SD	0.18	0.03	0.10	0.04	0.01	0.01	0.04	0.23	0.11	0.01	0

The mean values and standard deviations (SD) are also given. Total iron is expressed as FeO. Original, non-normalised data, together with analysis results of secondary standards, are available in S1.

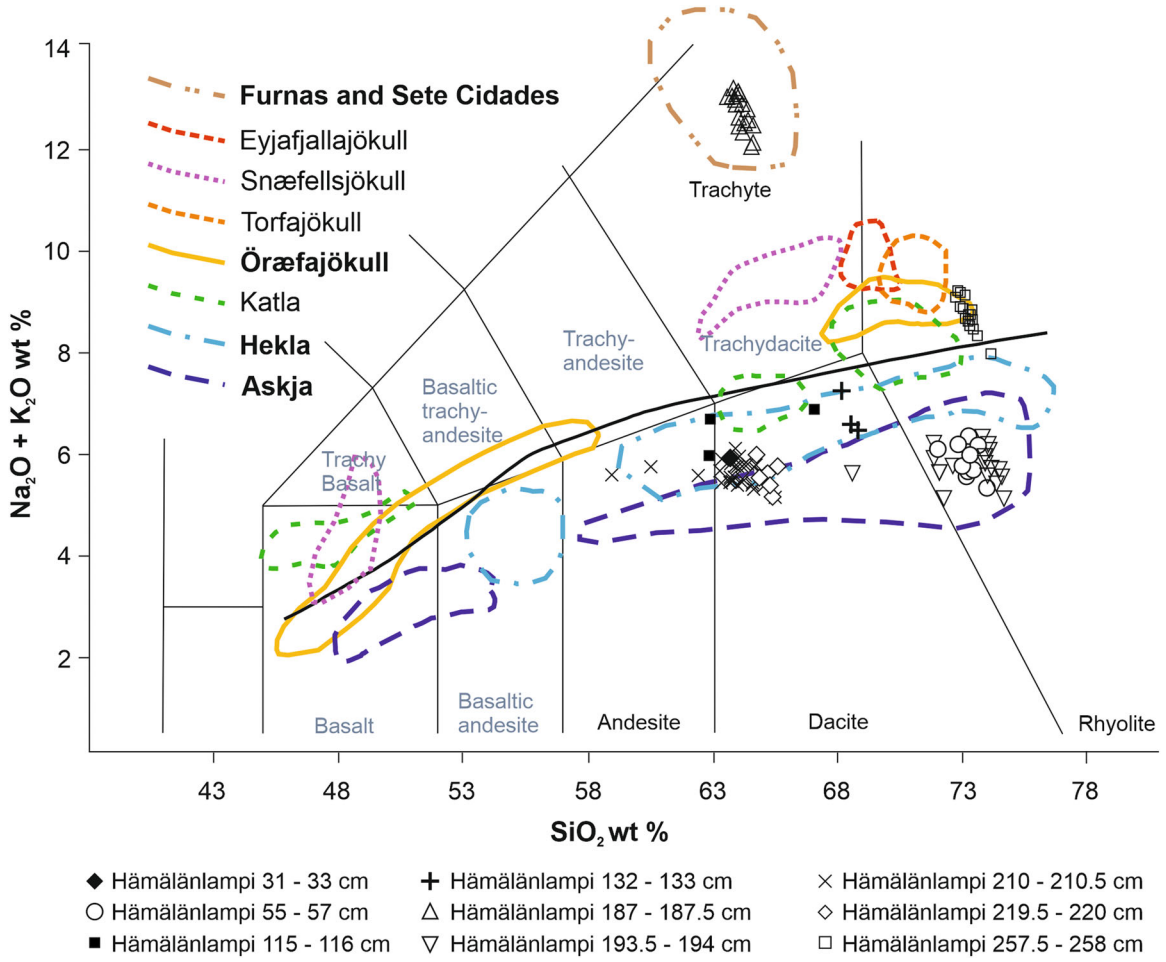

Figure 3. EPMA results of Hämälänlampi cryptotephra deposits plotted on a total alkali–silica (TAS) diagram. The black line represents the Kuno line separating low- and high-alkali products (Kuno, 1966). The volcanic rock classification is from Le Bas et al. (1986). Geochemical envelopes for the Furnas and Sete Cidades volcanoes (Azores), and Icelandic, silicic tephra-producing volcanic systems are shown. Data for the Azorean volcanoes are from Wastegård et al. (2020) and data for the Icelandic volcanoes are from Prestvik (1985); Steinthorsson et al. (1985); Larsen et al. (1999, 2001, 2002); Eiríksson et al. (2004); Sverrisdottir (2007); Guðmundsdóttir et al. (2011); Óladóttir et al. (2011); and Kalliokoski et al. (2019, 2020, 2023). All the data are normalised. [Color figure can be viewed at wileyonlinelibrary.com]

Hekla 1158 (Häm 132–133 cm)

At 132–133 cm sediment depth, a cryptotephra deposit comprising of vesicular colourless glass shards was identified (d in Fig. 2(D)). Geochemical characterisation of this deposit succeeded only for two shards due to the highly vesicular nature of the volcanic glass and a very low shard concentration (8 shards/g dry sediment). The results reveal this cryptotephra to be a Hekla dacite with a SiO_2 content ~68 wt % (Fig. 3).

Despite the low number of successful analyses, this deposit can be correlated to the Hekla 1158 eruption, the only historical Hekla eruption that produced dacitic tephra with a SiO_2 content >66 wt % (e.g., Larsen et al., 1999). The Hekla 1158 tephra has a distinct geochemical fingerprint among the historical intermediate Hekla tephras with its low FeO_{tot} and TiO_2 contents (Fig. 4(B); Larsen et al., 1999). Further support for the correlation is provided by previous identifications of this tephra at three peatland sites in Finland (Kalliokoski et al., 2020, 2023). The varve chronological age of the Hekla 1158 tephra in Hämälänlampi is 1155–1174 (−10/+8) CE. It is the oldest of the historical cryptotephras in Hämälänlampi, providing a useful check-point for confirming the accuracy of the newly constructed varve chronology.

Furnas C (Häm 187–187.5 cm)

The cryptotephra deposit at 187–187.5 cm depth comprises of colourless, vesicular volcanic glass shards (e in Fig. 2(D)). Despite the low shard concentration (15 shards/g dry sediment), EPMA was successful on 20 shards. The results reveal a trachytic composition with a SiO_2 range of 63.71–64.63 wt % and high alkali ($Na_2O + K_2O$) values between 12.08 and 13.14 wt % (Table 2; Fig. 3). This composition excludes an Icelandic origin, and plotting of the results on a TAS diagram reveals clear differences between this cryptotephra and, for example, the trachydacitic products of the Snæfellsjökull central volcano (Fig. 3). We correlate this deposit to the Furnas volcano in the Azores based on its geochemistry (Figs. 3 and 4(D)). Furthermore, both the geochemical composition (Fig. 4(D)) and the varve age (10 BCE–14 CE (−22/+12)) of the Furnas cryptotephra in Hämälänlampi support a correlation to the Furnas C tephra, which has been shown to differ from the other Furnas tephras with its lower FeO, TiO_2 and K_2O values (Wastegård et al., 2020; Fig. 4(D)).

The Furnas C eruption (1870 ± 120 ^{14}C BP) was the largest explosive eruption of Furnas during the past 5600 years (Guest et al., 1999; Cole et al., 1999), and isopach maps have revealed a northerly tephra dispersal (Guest et al., 1999), which explains the presence of the Furnas C tephra in Hämälänlampi,

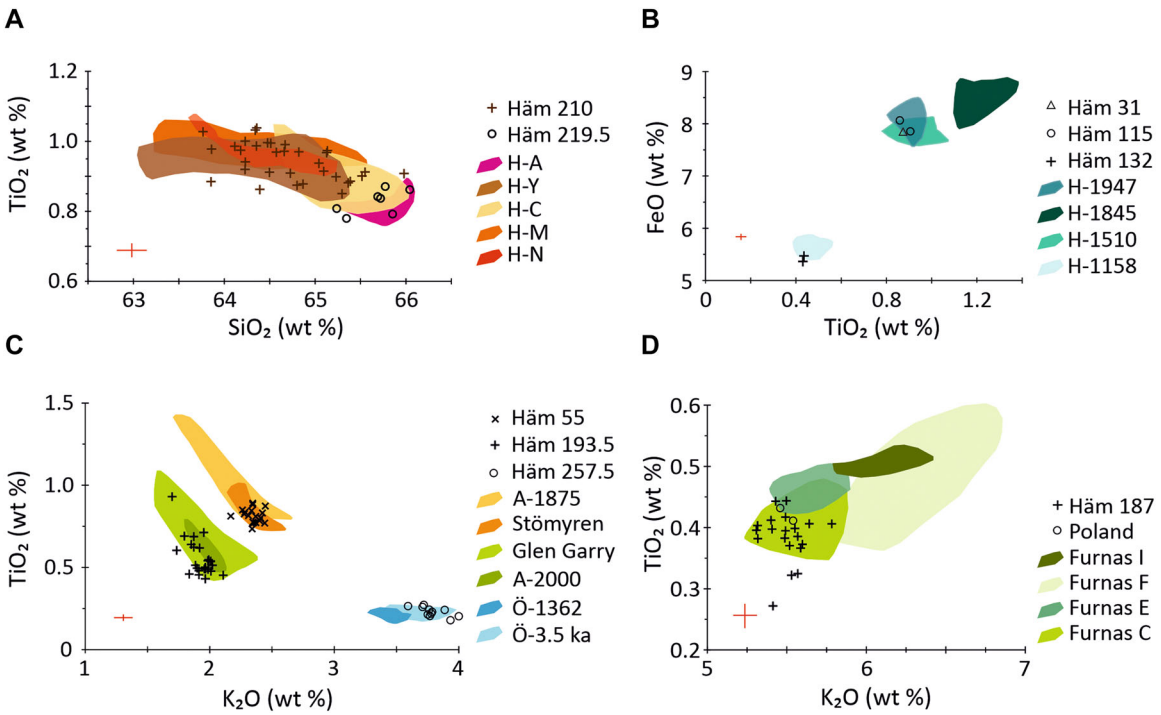

Figure 4. EPMA results of Hämälänlampi cryptotephra deposits compared against geochemical envelopes of the volcanic products of the most likely source eruptions. (A) A bivariate plot of TiO_2 and SiO_2 for the two-coloured Hekla tephras. (B) FeO:TiO_2 ratio in the historical Hekla tephras. (C) Comparison of TiO_2:K_2O content in Askja and Öræfajökull tephras. (D) A bivariate plot showing the TiO_2:K_2O content of the Furnas volcanic glass. Data for the geochemical envelopes from proximal tephra records: A-1875 (Larsen et al., 1999), A-2000 (Óladóttir et al., 2011), H-1947, H1510 and H-1158 (Larsen et al., 1999), H-1845 (Kalliokoski et al., 2020), H-A, H-Y, H-C, H-M, and H-N (Óladóttir et al., 2011; Meara et al., 2020; Kalliokoski et al., 2023), Furnas (Johansson et al., 2017; Wastegård et al., 2020), Ö-1362 (Larsen et al., 1999) and Ö-3.5 ka (Guðmundsson, 1998). Data for the geochemical envelopes from distal tephra records: H-1947 (Kalliokoski et al., 2020), A-1875 (Kalliokoski et al., 2019), Stömyren (Wastegård, 2005), Glen Garry (Barber et al., 2008), H-Y (Kalliokoski et al., 2023) and Ö-3.5 ka (Kalliokoski et al., 2023); data for the Furnas cryptotephra in Poland (lake Zabińskie) are from Kinder et al. (2020). All the data are normalised. The red error bars represent two standard deviations of repeated analysis of the Lipari secondary standard. [Color figure can be viewed at wileyonlinelibrary.com]

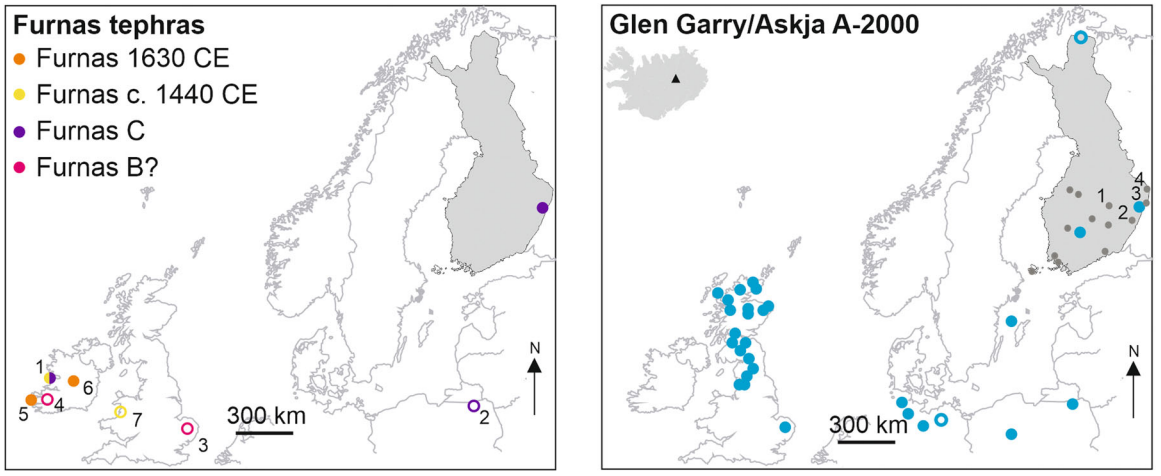

Figure 5. Distal occurrences of the Furnas tephras and the Glen Garry/Askja A-2000 tephra. Tentative correlations based on just one to two analysis points are marked with open circles. Note that the geochemical composition of proximal Furnas B tephra has not been analysed/published yet. Data sources for the Furnas tephras: (1) An Loch Mór, Chambers et al. (2004) (2) Lake Zabinskie, Kinder et al. (2020) (3) Diss Mere, Walsh et al. (2021) (4) Derrycunihy, Reilly and Mitchell (2015) (5) Portmagee, Hall and Pilcher (2002) (6) Mongan, Plunkett and Pilcher (2018) (7) Cors Fochno, Watson et al. (2017). Data sources for the Glen Garry tephra: Dugmore et al. (1995); Pilcher and Hall (1996); van den Bogaard and Schminke (2002); Langdon and Barber (2004); Barber et al. (2008); Tipping et al. (2008); Housley et al. (2014); Watson et al. (2016); Wulf et al. (2016); Garova (2020); Kinder et al. (2020); Martin-Puertas et al. (2021); Carter-Champion et al. (2025); and Müller et al. (2025). The filled grey circles on the Glen Garry dispersal map mark sites of previous cryptotephra studies in Finland (Kalliokoski et al., 2023). The numbered sites are (1) Kallio-Kourujärvi, (2) Punkaharju, (3) Parkusuo and (4) Hanhisuo. [Color figure can be viewed at wileyonlinelibrary.com]

c. 4600 km NE of the volcano. Tephra from historical eruptions of the Furnas volcano has also been identified in Northern Europe (Fig. 5); for example, cryptotephra deposits at Portmagee (Hall and Pilcher, 2002) and Mongan (Plunkett and Pilcher, 2018) in Ireland have been correlated to the 1630 CE eruption of Furnas (Reilly and Mitchell, 2015; Plunkett and Pilcher, 2018).

Glen Garry (Häm 193.5–194 cm)

The cryptotephra deposit at 193.5–194 cm sediment depth consists of scarce (32 shards/g dry sediment), colourless, vesicular shards (f in Fig. 2(D)). The EPMA results from 25 volcanic glass grains show a rhyolitic composition (SiO_2

68.65–74.62 wt %) and an origin in the Askja central volcano (Fig. 3; Table 2). This deposit can be correlated to the Glen Garry/Askja ~2000 cal a BP tephra (e.g., Dugmore and Newton, 1992; Guðmundsdóttir et al., 2016) based on its geochemical composition and stratigraphic position. Two distally transported Askja cryptotephra horizons of similar age have been identified in northern Europe, the Glen Garry and the Stömyren tephra (Wastegård, 2005), both of which have already previously been found in Finland (Garova 2020; Kalliokoski et al., 2023). These two can be separated mainly on the basis of their K_2O and TiO_2 contents, and the cryptotephra deposit in Hämälänlampi with its $K_2O < 2$ wt % and $TiO_2 < 0.75$ wt % clearly falls in the geochemical envelope of the Glen Garry tephra (Fig. 4(C)).

The Glen Garry tephra is an important marker horizon in the UK, where it has been identified in Scotland (Dugmore et al., 1995; Barber et al., 2008) and northern England (Pilcher and Hall, 1996). The Glen Garry tephra has also been found at many sites in mainland Europe, in Poland (Housley et al., 2014; Kinder et al., 2020) and Germany (van den Bogaard and Schminke, 2002; Wulf et al., 2016). Our results and the recent geochemically confirmed findings of the Glen Garry tephra in the Baltic Sea (Müller et al., 2025) and Finland (Garova, 2020; Carter-Champion et al., 2025) widen its known dispersal area (Fig. 5) and strengthen its role as an important interregional correlation horizon in northern Europe. The Hämälänlampi varve chronology provides a new, precise age of 131–115 (−22/+12) BCE for the Glen Garry/Askja ~2000 cal a BP tephra.

Hekla Y (Häm 210–210.5 cm)

Shard concentration of this cryptotephra deposit at the sediment depth of 210–210.5 cm is the highest one in Hämälänlampi (805 shards/g dry sediment). The deposit consists of brownish, vesicular volcanic glass shards (g in Fig. 2(D)). EPMA was successful on 34 shards, and the results place this cryptotephra in the andesitic/dacitic geochemical envelope of Hekla (Fig. 3). This cryptotephra horizon originates in one of the 10 eruptions that produced the ca. 2200–3000 years old, two-coloured Hekla tephra series (Larsen et al., 2020) consisting of tephras that share a similar geochemical composition. These tephras were first suggested to be impossible to distinguish from each other (Meara et al., 2020), but slight differences between them have been noted in other studies (Larsen et al., 2020; Kalliokoski et al., 2023).

Cryptotephra deposits in three Finnish sites have previously been correlated to one of the two-coloured Hekla tephras, namely, the Hekla Y (Kalliokoski et al., 2023), which has a soil accumulation rate (SeAR) age range of 2490–2720 BP (770–540 BCE) in Iceland (Larsen et al., 2020). In Finland, the Hekla Y tephra has been ^{14}C-dated to 2582 ± 142 cal a BP (774–490 BCE) (Kalliokoski et al., 2023). The varve age 509–493 (−23/+12) BCE of the cryptotephra deposit in Hämälänlampi suggests this tephra to originate from the Hekla A (c. 2420 cal a BP; 470 BCE, Larsen et al., 2020) rather than the Hekla Y eruption (Fig. 6). However, the cryptotephra in Hämälänlampi has higher TiO_2 (0.9–1.0 wt %), FeO_{tot} (~6.8% wt %) and MgO (~1.44 wt %) contents than Hekla A ($TiO_2 < 0.9$ wt %, FeO_{tot} ~6.5 wt % and MgO ~1.2 wt % from Meara et al., 2020), and shows a closer affinity to the Hekla Y tephra (Fig. 4(A) and Figure 1 in Supplementary material S1).

In general, correlating the two-coloured Hekla tephras to their source eruptions is a difficult task when their age differences are small (even as small as 20 years), error margins in age determinations are large (200–300 years for ^{14}C ages) and geochemical compositions are nearly identical (Figs. 6 and 4(A)). Additionally, the zoned magma chamber of Hekla can produce tephra with a wide geochemical range during a single eruption (e.g., Sigmarsson et al., 1992; Sverrisdóttir, 2007). The full range of the erupted products is generally present only at proximal sites, and may need to be pieced together from investigations at several sites due to shifting wind directions during an eruption (Jónsson et al., 2020). Furthermore, the slight differences in the geochemical composition of the Hekla tephras may be detected only when samples with similar SiO_2 values are compared (e.g., Kalliokoski et al., 2023). Therefore, if the proximal and distal records contain tephra from different eruption phases, and the full range of erupted products remains unknown, establishing robust correlations for the two-coloured Hekla tephras may be impossible based on the major element geochemistry alone.

At this stage, we suggest a correlation to Hekla Y for the cryptotephra deposit in Hämälänlampi despite its younger varve age. However, a correlation to Hekla A cannot be ruled out completely, since the proximal geochemistry of the Hekla A tephra has been published from just one site (Meara et al., 2020) and further studies are necessary for determining the full geochemical range of the Hekla A tephra. If our correlation is correct, it strengthens the status of Hekla Y as one of the most prominent cryptotephra deposits in Finland (Kalliokoski et al., 2023). Hekla Y has the potential to become an important correlation horizon in Finland and northern Fennoscandia, especially with reference to the limited dispersal of the major Hekla tephras H-3, H-S and H-4 to Finland (Kalliokoski et al., 2023).

Hekla C? (Häm 219.5–220 cm)

The cryptotephra deposit at 219.5–220 cm depth, consisting of yellow and brown vesicular volcanic glass, has a low shard concentration (34 shards/g dry sediment). The electron microprobe analyses of seven shards reveal an andesitic–dacitic Hekla composition (Fig. 3; Table 2). The geochemistry of this cryptotephra deposit differs from the Hekla tephra at 210–210.5 cm depth based on its lower TiO_2 (0.78–0.87 wt %) and FeO (6.15–6.44 wt %) contents (Fig. 4(A); Table 1). Varve chronology constrains the age of this cryptotephra to 735–720 (−24/+12) BCE, c. 211–242 years older than the varve age of Hekla Y in Hämälänlampi. On the one hand, comparisons with SeAR ages of the two-coloured Hekla series at proximal sites indicate this tephra to originate most likely in the Hekla Y, Z, B or C eruption (Fig. 6). On the other hand, most likely candidates based on eruption size and the easterly, south-easterly direction of dispersal axes in the proximal area are Hekla M (uncompacted volume 0.437 km^3) and Hekla N (uncompacted volume 0.696 km^3) eruptions (Larsen et al., 2020). However, geochemical comparisons between all the two-coloured Hekla tephra layers from the proximal region (Larsen et al., 2020; Meara et al., 2020) and Häm-220 as well as the varve age suggest that this deposit originates from the Hekla C eruption (Fig. 4(A)). Hekla B, Z, M and N tephras in the proximal sites have a TiO_2 content of 0.9–1.0 wt % (Meara et al., 2020; Kalliokoski et al., 2023), whereas the TiO_2 content in Hekla C and Häm-220 is generally lower: 0.8–0.9 wt %.

The Hekla C eruption was relatively large (0.545 km^3 uncompacted volume), with the main dispersal direction towards north–northwest in Iceland (Larsen et al., 2020). However, the proximal dispersal axis of a tephra is not necessarily a reliable determinant of its representation in the distal records, as is shown by the identification of, for example, Hekla 1104, Torfajökull–Landnám and Hekla 4 in Finland (Kalliokoski et al., 2023). All these eruptions had a northerly

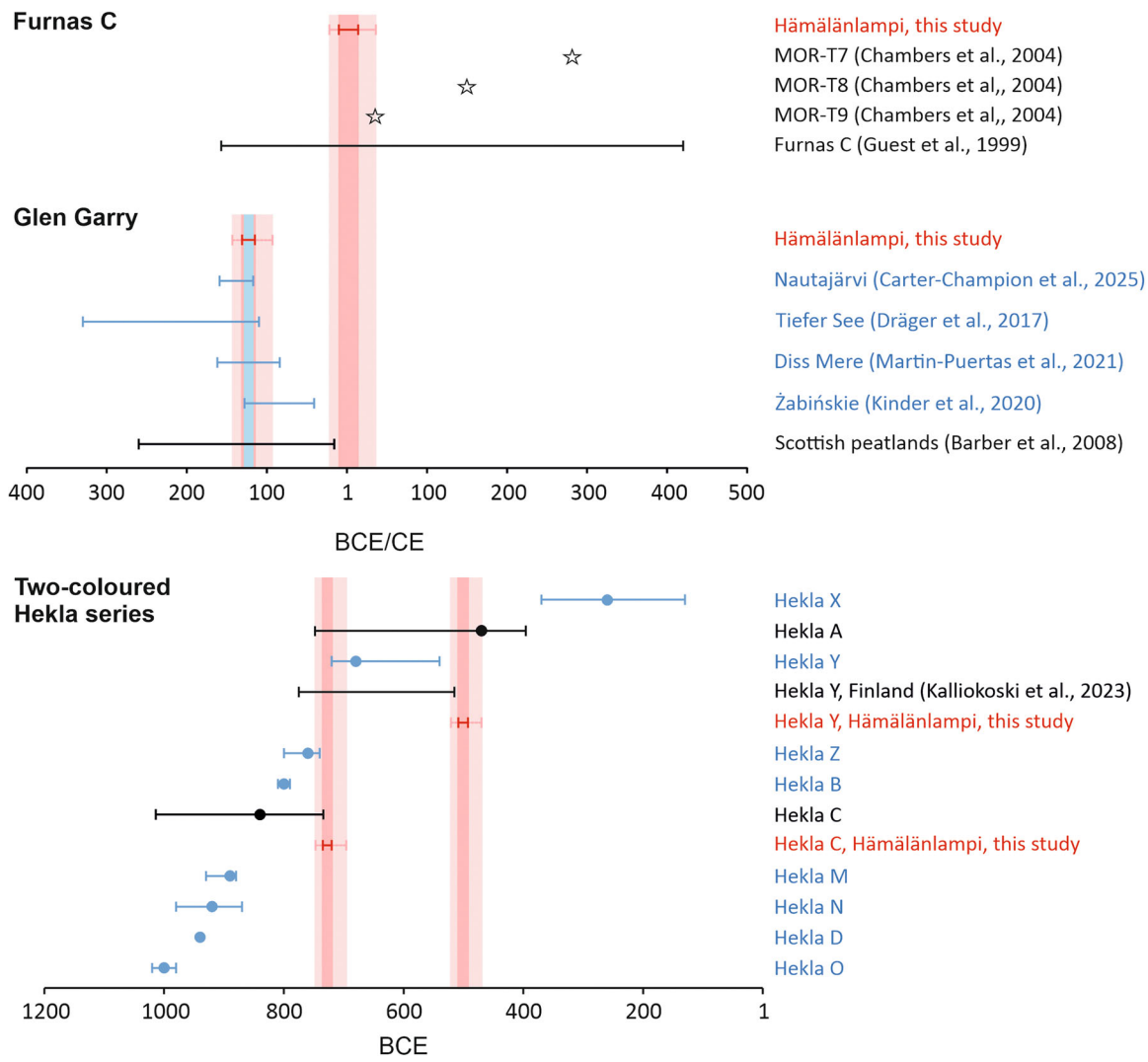

Figure 6. Comparison of the new varve ages and previous age estimates of the tephras present in Hämälänlampi. The varve ages from Hämälänlampi are marked in dark red and varve count uncertainties are shown in light red colour. Previously published ^{14}C ages were calibrated in the OxCal 4.4 online programme (Bronk Ramsey, 2009) using the IntCal-20 calibration curve (Reimer et al., 2020). The calibrated ^{14}C ages are marked with black lines, whereas blue lines mark previously published varve ages of the Glen Garry tephra, and soil accumulation rate-based ages of the Hekla tephras. Filled circles represent best age estimates for the Hekla tephras (Larsen et al., 2020). A new, integrated varve age for the Glen Garry tephra (128–117 BCE) is shown as a blue field that overlaps exactly with the new varve age from Hämälänlampi. The stars denote the ages of the MOR tephra layers at An Loch Mór (Chambers et al., 2004). [Color figure can be viewed at wileyonlinelibrary.com]

Table 3. New varve ages from Hämälänlampi, and previously published age estimates for the prehistoric cryptotephras present in Hämälänlampi.

Tephra	Previous age estimates	Age in CE/BCE	Reference	New varve age	Varve count uncertainty
Furnas C	1870 ^{14}C ± 120 BP	157 BCE–420 CE	Guest et al. (1999)	10 BCE–14 CE	−22/+12
Glen Garry	2210–1966 BP	260–16 BCE	Barber et al. (2008)	131–115 BCE	−22/+12
Glen Garry	94 + 34/−53 CE	128–41 BCE	Kinder et al. (2020)		
Glen Garry	2073 ± 39 BP	162–84 BCE	Martin-Puertas et al. (2021)		
Glen Garry	2088 ± 21 BP	159–117 BCE	Carter-Champion et al. (2025)		
Glen Garry	2170 ± 110 BP	330–110 BCE	Wulf et al. (2016), Dräger et al. (2017)		
Hekla Y	2540–2770 b2k	770–540 BCE	Larsen et al. (2020)	509–493 BCE	−23/+12
Hekla Y	2489 ± 28 ^{14}C BP	775–515 BCE	Kalliokoski et al. (2023)		
Hekla C	2660 ± 80 ^{14}C BP	1014–734 BCE	Larsen et al. (2020)	735–720 BCE	−24/+12
Öræfajökull 3.5 ka	3292 ± 27 ^{14}C BP	1616–1506 BCE	Kalliokoski et al. (2023)	1531–1512 BCE	−32/+13

The radiocarbon ages have been calibrated using the OxCal 4.4 online programme (Bronk Ramsey, 2009) and the IntCal-20 calibration curve (Reimer et al., 2020).

direction of tephra dispersal in Iceland. With reference to the chronological and geochemical complications of correlating the two-coloured Hekla tephras to their source eruptions, we suggest only a tentative correlation to the Hekla C eruption for this cryptotephra.

Häm 257.5–258 cm

The oldest cryptotephra deposit in Hämäläänlampi has 30 shards/g dry sediment. The shards are colourless, with platy and vesicular morphology. EPMA results from 11 glass shards indicate Öræfajökull as the source volcano for this rhyolitic high-alkali cryptotephra (Fig. 3; Table 2). The varve age of this deposit in Hämäläänlampi is 1531–1512 (−32/+13) BCE. Its geochemical composition with high total alkalis ($Na_2O + K_2O > 8$ w%) and characteristic, low MgO (<0.03 wt %) reveals a perfect correlation with the Öræfajökull 3.5 ka tephra that was first described from a proximal site close to Vatnajökull in Iceland (Guðmundsson, 1998) and later ^{14}C dated to 3510 ± 55 cal a BP (1616–1506 BCE) at a soil section in Vopnafjörður, NE Iceland (Table 3; Kalliokoski et al., 2023). This tephra has previously been found as a cryptotephra deposit at the Haapasuo peatland site in central Finland and as a single shard in a mixed deposit at Kivihypönneva peatland in western Finland (Kalliokoski et al., 2023). The geochemical compositions of the Öræfajökull 1362 tephra and the Öræfajökull 3.5 ka tephra identified in Iceland, the Finnish peatlands and Hämäläänlampi are nearly identical (Fig. 4(C)). The new finding presented here is an important addition to the Northern European tephrochronological framework, as it confirms the status of the Öræfajökull 3.5 ka tephra as a regional high-resolution dating horizon with a distinct geochemical signature.

Discussion

New varve ages for the Furnas C and Glen Garry/Askja 2000 tephras

The Furnas C tephra

The suggested, new varve age 10 BCE–14 CE (−22/+12) for Furnas C tephra is a great improvement from the previous best age estimate of 1870 ^{14}C ± 120 BP (157 BCE–420 CE) by Guest et al. (1999) (Table 3; Fig. 6). This new, high-precision age can be used for revisiting previous correlations of cryptotephra deposits to the Furnas volcano. For example, three cryptotephra deposits at An Loch Mór, western Ireland—MOR-T7 (c. 1670 cal a BP; 280 CE), MOR-T8 (c. 1800 cal a BP; 150 CE) and MOR-T9 (c. 1915 cal a BP; 35 CE) (Chambers at el., 2004)—have recently been suggested to originate from the Furnas volcano on geochemical grounds (Johansson et al., 2017; Wastegård et al., 2020). However, due to their identical geochemistry and fairly similar ages, it has not been possible to determine which one of the MOR cryptotephra deposits, if any, correlates to the Furnas C eruption. The new varve age of Furnas C from Hämäläänlampi aligns perfectly with the age of MOR-T9 (Fig. 6), supporting a correlation of MOR-T9 to Furnas C.

Other prehistoric Furnas cryptotephra findings come from lake Żabińskie in Poland (Kinder et al., 2020) and lake Diss Mere in England (Walsh et al., 2021; Fig. 5). These cryptotephras have tentatively been correlated to the Furnas C (Żabińskie) and Furnas B (Diss Mere) eruptions based on analyses of just a couple of shards. The age estimate of the Furnas B eruption is 2310 ^{14}C ± 160 BP; 800–34 cal BCE (Guest et al., 1999). A cryptotephra deposit (c. 465–365 cal BCE) from a woodland hollow at Derrycunihy (Reilly and Mitchell, 2015) has also been suggested to correlate to the Furnas B eruption (Wastegård et al., 2020). However, the lack of proximal geochemical data for the Furnas B tephra complicates these correlations. In lake Żabińskie, the Glen Garry and Furnas cryptotephras co-occur within 2 cm of turbidite sediment, where the Glen Garry tephra is partly mixed into the Furnas tephra immediately below. The new results from Hämäläänlampi place the Furnas C tephra stratigraphically above the Glen Garry tephra and reveal just around a 120-year age difference between the two (Supplementary material S1). Therefore, it is likely that the stratigraphical order of these two cryptotephras in Żabińskie has been disturbed by the redepositional processes recognised in Kinder et al. (2020). The geochemical compositions of the Furnas cryptotephra deposits in Żabińskie and Hämäläänlampi are identical (Fig. 4(D)), and the new varve age of the Furnas C cryptotephra supports the correlation of the cryptotephra in Żabińskie to the Furnas C eruption instead of the c. 400 years older Furnas B eruption. For the possible Furnas cryptotephra in Diss Mere, an origin in the Furnas C eruption can be excluded based on its occurrence well below the Glen Garry tephra.

Glen Garry tephra

The previous, best age estimates for the Glen Garry tephra are shown in Table 3 and Fig. 6. The most precise ^{14}C age (2176 cal. BP; 2210–1966 cal. BP 2σ range) comes from a study by Barber et al. (2008), who dated the cryptotephra isochron at eight Scottish peatland sites by AMS^{14}C and integrated their results using Bayesian age–depth modelling. Varve ages for the Glen Garry tephra have been obtained from the floating varve chronology of Diss Mere in England (Martin-Puertas et al., 2021) and the partially varved sediment core from lake Tiefer See in Germany (Dräger et al., 2017), as well as from the continuously varved lake Nautajärvi in Finland (Carter-Champion et al., 2025). Additionally, Kinder et al. (2020) have identified the Glen Garry tephra as a cryptotephra horizon in a varved lake Żabińskie, Poland.

Integration of all the independent varve ages for the Glen Garry tephra (Fig. 6) results in a new high-resolution age of 128–117 BCE (2078–2067 varve years BP). Here, the most probable age is the interval between the youngest (from Nautajärvi) and the oldest (from Żabińskie) possible varve age, when all published varve-based ages with their age uncertainties are considered equally reliable (Fig. 6). The new, integrated varve age for Glen Garry is a perfect match with the varve age 131–115 −22/+12 BCE (2081–2065 varve years BP) from Hämäläänlampi (Fig. 6).

Hämäläänlampi as a cryptotephra archive

Hämäläänlampi has the highest number of geochemically identified cryptotephra horizons of any Finnish site thus far, which indicates Hämäläänlampi to be an efficient cryptotephra trap. The relatively high organic content of the sediment (LOI up to 50%) enables the detection and extraction of even the smallest amounts of cryptotephra, while the continuous varve formation/preservation and stratigraphically well-confined cryptotephra deposits are ideal for high-resolution dating of prehistoric tephra horizons.

Only two other Finnish varved lakes, Kallio-Kourujärvi (Kalliokoski et al., 2019) and Nautajärvi (Carter-Champion et al., 2025), have been previously investigated for the presence of cryptotephra, and the results reveal clear differences between them as cryptotephra archives. In Kallio-Kourujärvi, only the Askja 1875 tephra was detected in the 3000-year biogenic varve record, where it forms a well-confined horizon in 1 cm of sediment representing 11

varve years (Kalliokoski et al., 2019). In Nautajärvi, 31 cryptotephra peaks were counted from selected intervals of the c. 9900-year clastic–biogenic varve record, and nearly every centimetre of the investigated sediment was reported to contain cryptotephra (Carter-Champion et al., 2025). However, only five cryptotephra peaks could be correlated to source eruptions, and the cryptotephra deposits were reported to be generally heterogeneous (Carter-Champion et al., 2025). The majority of the tephra peaks and the background input consist of Vedde Ash-like volcanic glass that has been reworked and redeposited into the deepest part of the lake basin for over 7000 years (Carter-Champion et al., 2025).

In comparison to Kallio-Kourujärvi and Nautajärvi, Hämälänlampi appears to be exceedingly valuable as a cryptotephra archive. First, the number of cryptotephra deposits in Hämälänlampi is high. Eight cryptotephra horizons have been deposited in Hämälänlampi during the past 3000 years, whereas Kallio-Kourujärvi, located 180 km west of Hämälänlampi (site 1 in Fig. 5), contains just one cryptotephra over the same time period. Second, in contrast to Nautajärvi, no background input of volcanic glass, repeating tephra geochemistry or heterogeneous cryptotephra deposits are observed in Hämälänlampi, which makes the tephrostratigraphy robust. At present, the number of tephrochronological studies from Finnish varve records is too low for a detailed discussion on the reasons for the highly variable quality of the varve records as cryptotephra archives. However, the differences between the studied records highlight the need for continued cryptotephra studies to identify the factors that influence cryptotephra deposition, reworking and detection in varve records.

Tephra dispersal in Finland

Hämälänlampi is one of the easternmost sites investigated for the presence of cryptotephra in Finland and, as such, a valuable site for refining tephra dispersal maps. The results confirm that the Icelandic Hekla 1510, Hekla 1158, Glen Garry and Öræfajökull 3.5 ka tephras were dispersed even further east than previously known. Additionally, the new results, together with earlier observations (Kalliokoski et al., 2023), indicate that, surprisingly, the Hekla Y tephra originating in a moderate-sized eruption is the most prominent cryptotephra layer in Finnish sites. The high shard concentration and the relatively large shards (Kalliokoski et al., 2023) imply that the weather conditions during the Hekla Y eruption have been exceptionally favourable for eastwards ash dispersal and fall-out in Finland.

The results further confirm the earlier observations regarding the absence or very limited dispersal of the major Hekla tephras, H-3 (3295 ± 95 varve years BP in Zillén et al., 2002) and H-4 (GIC age 4325 ± 8 a b1.95k in Davies et al., 2024), in Finland. H-3 has been reported from several sites in Sweden (e.g., Zillén et al., 2002; Bergman et al., 2004; Watson et al., 2016), but it has not been found in Finland. The H-4 tephra has been identified only at three sites in western Finland, where it forms deposits with very low shard concentrations (Kalliokoski et al., 2023; Carter-Champion et al., 2025). The limited occurrence of H-4 in Finland is surprising, as it has one of the widest dispersal areas of the Holocene tephras in northern Europe (e.g., Kalliokoski et al., 2023), and is the most common prehistoric tephra in Sweden (Wastegård, 2005).

In addition to the Icelandic tephras, ultra-distal cryptotephras sourced from other volcanic regions have been identified in Finland. These include the Alaskan WRAe and Aniakchak tephras (Kalliokoski et al., 2023) and the Kamchatkan KS_2 tephra (Carter-Champion et al., 2025). The identification of Furnas C in Hämälänlampi confirms that tephra from the Azores can be transported to Finland and form detectable cryptotephra horizons. Furnas C is the only non-Icelandic tephra found in Hämälänlampi and, thus far, WRAe is the only ultra-distal cryptotephra that has been identified in more than one site in Finland (Kalliokoski et al., 2023), which indicates an extremely patchy occurrence of ultra-distal tephras in Finland.

The new results from Hämälänlampi increase the number of geochemically confirmed cryptotephras in the Finnish tephrochronology to 23 and reveal that the occurrence frequency of tephra in environmental archives in Finland remains similar across the country from west to east. Fifteen cryptotephras have been identified in western Finland and 14 in eastern Finland. Even if some tephras seem to be restricted to either the western (Hekla 1104 and Hekla 4) or the eastern (Torfajökull–Landnám, Hekla Y and Öræfajökull 3.5 ka) half of the country, the tephra occurrence is remarkably patchy (Kalliokoski et al., 2023). For example, only two of the nine cryptotephra deposits in Hämälänlampi—Askja 1875 and Hekla Y—are present in the previously investigated Kallio-Kourujärvi lake (site 1 in Fig. 5) or the nearby Punkaharju, Parkusuo and Hanhisuo peatland sites (sites 2, 3 and 4 in Fig. 5). Furthermore, the 877 ± 2 CE Torfajökull–Landnám and the 852 ± 2 CE White River Ash identified at Hanhisuo (Kalliokoski et al., 2023) are absent from Hämälänlampi. The differences between the tephrostratigraphies at Hämälänlampi and the peatland sites in eastern Finland are noteworthy, since peatlands have been demonstrated to generally contain more complete tephrostratigraphies than lakes (Watson et al., 2016).

The general trend of missing cryptotephra horizons in lake sediments (Watson et al., 2016) could be explained partly by the easier detection of even minor amounts of volcanic glass embedded in an organic peat matrix. However, tephra concentrations in environmental records are influenced by multiple factors in addition to the amount of primary fall-out. For lake sediments, shard delivery from the catchment area and basin processes may affect the shard distribution and maximum shard concentrations (Davies et al., 2007; Pyne-O'Donnell, 2011; Boygle, 1999). In peatlands, tephra shards can be remobilized and redeposited both by wind and water action on the peat surface, and by flowing water deeper in the mire (Persson, 1966; Boygle, 1999; Bergman et al., 2004). When the amount of primary tephra fall-out is small, the number of cryptotephra shards may remain below the detection limit even in peatlands due to the redistribution of the shards. An example of this is the Hekla 1947 tephra, which has not yet been found in Finnish peatlands within the fall-out zone that was determined based on eye-witness reports in 1947 (Salmi, 1948; Kalliokoski et al., 2019, 2020).

The tephra shard concentrations in Finland are generally very low (Fig. 2; Kalliokoski et al., 2023), and the majority of the deposits are most likely near the detection limit, which could explain the patchiness in the dispersal maps. Here, the properties of the embedding matrix may play a substantial role in the detection of cryptotephra. For example, the sediment in Hämälänlampi has a high organic content, which enables efficient detection of cryptotephra shards after combustion. Additionally, the cryptotephra deposits can be assumed to consist of a combination of direct fall-out on the lake and in-wash from the surrounding catchment, which increases the shard concentrations in the sediments. These factors may explain why more cryptotephra deposits are detected in Hämälänlampi than the nearby peatland sites.

Conclusions

We present a new varve chronology from eastern Finland for high-resolution paleoenvironmental studies. The results show

that varve formation and preservation in lake Hämälänlampi have been continuous for at least the past 4500 years. The varve chronology was constructed by counting varves from epoxy-embedded samples under a microscope, and high-resolution micro-XRF elemental maps were used as an additional aid in identifying the microscale sediment structures. The robustness of the varve chronology was evaluated by using the discovery, geochemical fingerprinting and correlation of historical cryptotephra deposits as an independent dating method.

Our results refine the Finnish tephrochronological framework with an addition of three new cryptotephra marker horizons, Hekla 1947, Furnas C and Hekla C, and improved age constraints for the Glen Garry, Hekla Y and Öræfajökull 3.5 ka tephra. The geochemical identification of prehistoric cryptotephras in varved lacustrine sediments greatly improves the previous estimates of source eruption ages and testifies to the significance of the continuous Finnish varve chronologies for precise age determinations of tephra layers and for improving our knowledge on the eruption histories of their source volcanoes. However, our results also reveal complexities in correlating the geochemically similar, two-coloured Hekla tephras to their counterparts in proximal areas, even when a precise varve age is available.

The precision of the new, integrated high-resolution varve age of 128–118 BCE for the Glen Garry/Askja ~2000 tephra demonstrates the benefits of between-site comparisons of independently determined varve ages. Our results suggest that tephrochronological studies of the Northern European continuous varve records are critically important for improving the age constraints of prehistoric tephras absent from the Greenland ice core records. The new varve-based tephra ages and geochemical data on volcanic glass composition from Hämälänlampi provide excellent points of comparison for future studies and for refining the tephra ages further as new cryptotephra findings are obtained from varve records.

Supporting information

Additional supporting information can be found in the online version of this article.

Supplementary Information

Acknowledgements. We thank Timo Saarinen for his help in the early stages of this research project and Tapio Suominen for assistance in lake coring. We acknowledge financial support from the Academy of Finland (grant no. 339789) and Maa- ja vesitekniikan tuki ry. Open-access publishing was facilitated by Turun yliopisto, as part of the Wiley–FinELib agreement. Open access publishing facilitated by Turun yliopisto, as part of the Wiley - FinELib agreement.

Data Availability Statement

The data set that supports the findings of this study is available in the supplementary material of this article.

References

Abbott, P.M. & Davies, S.M. (2012) Volcanism and the Greenland ice-cores: the tephra record. *Earth-Science Reviews*, 115, 173–191.

Barber, K., Langdon, P. & Blundell, A. (2008) Dating the Glen Garry tephra: a widespread late-Holocene marker horizon in the peatlands of northern Britain. *The Holocene*, 18, 31–43.

Bas, M.J.L., Maitre, R.W.L., Streckeisen, A. & Zanettin, B. (1986) A chemical classification of volcanic rocks based on the total alkali–silica diagram. *Journal of Petrology*, 27, 745–750.

Bergman, J., Wastegård, S., Hammarlund, D., Wohlfarth, B. & Roberts, S.J. (2004) Holocene tephra horizons at Klocka Bog, west-central Sweden: aspects of reproducibility in subarctic peat deposits. *Journal of Quaternary Science*, 19, 241–249.

Billah, M., Tuovinen, N., Salminen, S., Tylmann, W., Kalliokoski, M. & Saarni, S. (2026) Varve record reveals rapid development of hypolimnetic anoxia in a Northern European lake resulting from urban activities. *Anthropocene*, 53, 100508.

van der Bilt, W.G.M., Lane, C.S. & Bakke, J. (2017) Ultra-distal Kamchatkan ash on Arctic Svalbard: towards hemispheric cryptotephra correlation. *Quaternary Science Reviews*, 164, 230–235.

van den Bogaard, C. & Schmincke, H.-U. (2002) Linking the North Atlantic to central Europe: a high-resolution Holocene tephrochronological record from northern Germany. *Journal of Quaternary Science*, 17, 3–20.

Bonk, A., Kinder, M., Enters, D., Grosjean, M., Meyer-Jacob, C. & Tylmann, W. (2016) Sedimentological and geochemical responses of Lake Żabińskie (north-eastern Poland) to erosion changes during the last millennium. *Journal of Paleolimnology*, 56, 239–252.

Borgmark, A. & Wastegård, S. (2008) Regional and local patterns of peat humification in three raised peat bogs in Värmland, south-central Sweden. *GFF*, 130, 161–176.

Boygle, J. (1999) Variability of tephra in lake and catchment sediments, Svínavatn, Iceland. *Global and Planetary Change*, 21, 129–149.

Boygle, J. (2004) Towards a Holocene tephrochronology for Sweden: geochemistry and correlation with the North Atlantic tephra stratigraphy. *Journal of Quaternary Science*, 19, 103–109.

Bronk Ramsey, C. (2009) Bayesian analysis of radiocarbon dates. *Radiocarbon*, 51, 337–360.

Candy, I., Boyall, L., Lincoln, P., Martin-Puertas, C., Matthews, I. & Holt-Wilson, T.et al. (2025) A cold but stable 4,200 yr event in Britain and the northeastern Atlantic region. *Quaternary Science Reviews*, 349, 109093.

Carter-Champion, A., Flowers, K., Ojala, A.E.K., Blockley, S., Lincoln, P., Zhang, S. et al. (2025) A tephrostratigraphic investigation of the continuously varved Holocene Boreal lake Nautajärvi, Finland, provides precise age estimate for Lairg A/Hekla 5 eruption. *Journal of Quaternary Science*, 40, 1212–1229.

Chambers, F.M., Daniell, J.R.G., Hunt, J.B., Molloy, K. & O'Connell, M. (2004) Tephrostratigraphy of An Loch Mór, Inis Oírr, western Ireland: implications for Holocene tephrochronology in the north-eastern Atlantic region. *The Holocene*, 14, 703–720.

Cole, P.D., Guest, J.E., Queiroz, G., Wallenstein, N., Pacheco, J.M., Gaspar, J.L. et al. (1999) Styles of volcanism and volcanic hazards on Furnas volcano, São Miguel, Azores. *Journal of Volcanology and Geothermal Research*, 92, 39–53.

Croudace, I.W., Löwemark, L., Tjallingii, R. & Zolitschka, B. (2019) Current perspectives on the capabilities of high resolution XRF core scanners. *Quaternary International*, 514, 5–15.

Czymzik, M., Dulski, P., Plessen, B., von Grafenstein, U., Naumann, R. & Brauer, A. (2010) A 450 year record of spring-summer flood layers in annually laminated sediments from Lake Ammersee (southern Germany). *Water Resources Research*, 46, W11528.

Davies, S.M. (2015) Cryptotephras: the revolution in correlation and precision dating. *Journal of Quaternary Science*, 30, 114–130.

Davies, S.M., Albert, P.G., Bourne, A.J., Owen, S., Svensson, A., Bolton, M.S.M. et al. (2024) Exploiting the Greenland volcanic ash repository to date caldera-forming eruptions and widespread isochrons during the Holocene. *Quaternary Science Reviews*, 334, 108707.

Davies, S.M., Elmquist, M., Bergman, J., Wohlfarth, B. & Hammarlund, D. (2007) Cryptotephra sedimentation processes within two lacustrine sequences from west central Sweden. *The Holocene*, 17, 319–330.

Dörfler, W., Feeser, I., van den Bogaard, C., Dreibrodt, S., Erlenkeuser, H., Kleinmann, A. et al. (2012) A high-quality annually laminated sequence from Lake Belau, Northern Germany: revised chronology and its implications for palynological and tephrochronological studies. *The Holocene*, 22, 1413–1426.

Dräger, N., Theuerkauf, M., Szeroczyńska, K., Wulf, S., Tjallingii, R., Plessen, B. et al. (2017) Varve microfacies and varve preservation

record of climate change and human impact for the last 6000 years at Lake Tiefer See (NE Germany). *The Holocene*, 27, 450–464.
Dugmore, A.J. & Newton, A.J. (1992) Thin tephra layers in peat revealed by X-radiography. *Journal of Archaeological Science*, 19, 163–170.
Dugmore, A.J., Larsen, ú & Newton, A.J. (1995) Seven tephra isochrones in Scotland. *The Holocene*, 5, 257–266.
Eiríksson, J., Larsen, G., Knudsen, K.L., Heinemeier, J. & Símonarson, L.A. (2004) Marine reservoir age variability and water mass distribution in the Iceland Sea. *Quaternary Science Reviews*, 23, 2247–2268.
Farnsworth, W.R., Aradóttir, N., Brynjólfsson, S., Eddudóttir, S.D., Erlendsson, E., Guðfinnsson, G.H. et al. (2025) Explosive volcanic history of Snæfellsjökull, West Iceland: geochemistry, chronology and tephra distribution. *Quaternary Science Reviews*, 359, 109346.
Garova, E. 2020. Cryptotephras in European Arctic: extending tephrochronology to northern Finland and Russia. MS Thesis in Geology. University of Iceland, 88.
Grönlund, E. & Asikainen, E. (1992) Reflections of slash-and-burn cultivation cycles in a varved sediment of lake Pitkälampi (North Karelia, Finland). *Laborativ Arkeologi*, 6, 43–48.
Gudmundsdóttir, E.R., Eiríksson, J. & Larsen, G. (2011) Identification and definition of primary and reworked tephra in Late Glacial and Holocene marine shelf sediments off North Iceland. *Journal of Quaternary Science*, 26, 589–602.
Gudmundsdóttir, E.R., Larsen, G., Björck, S., Ingólfsson, Ó. & Striberger, J. (2016) A new high-resolution Holocene tephra stratigraphy in eastern Iceland: improving the Icelandic and North Atlantic tephrochronology. *Quaternary Science Reviews*, 150, 234–249.
Guest, J.-E., Gaspar, J.L., Cole, P.D., Queiroz, G., Duncan, A.M., Wallenstein, N. et al. (1999) Volcanic geology of Furnas volcano, São Miguel, Azores. *Journal of Volcanology and Geothermal Research*, 92, 1–29.
Guilderson, T.P., Reimer, P.J. & Brown, T.A. (2005) The boon and bane of radiocarbon dating. *Science*, 307, 362–364.
Guðmundsson, H. 1998. Holocene glacier fluctuations and tephrochronology of the Öræfi district, Iceland. PhD thesis. University of Edinburgh, Edinburgh.
Hall, V.A. & Pilcher, J.R. (2002) Late-Quaternary Icelandic tephras in Ireland and Great Britain: detection, characterization and usefulness. *The Holocene*, 12, 223–230.
Haltia-Hovi, E., Nowaczyk, N. & Saarinen, T. (2011) Environmental influence on relative palaeointensity estimates from Holocene varved lake sediments in Finland. *Physics of the Earth and Planetary Interiors*, 185, 20–28.
Haltia-Hovi, E., Nowaczyk, N., Saarinen, T. & Plessen, B. (2010) Magnetic properties and environmental changes recorded in Lake Lehmilampi (Finland) during the Holocene. *Journal of Paleolimnology*, 43, 1–13.
Haltia-Hovi, E., Saarinen, T. & Kukkonen, M. (2007) A 2000-year record of solar forcing on varved lake sediment in eastern Finland. *Quaternary Science Reviews*, 26, 678–689.
Heiri, O., Lotter, A.F. & Lemcke, G. (2001) Loss on ignition as a method for estimating organic and carbonate content in sediments: reproducibility and comparability of results. *Journal of Paleolimnology*, 25, 101–110.
Housley, R.A., MacLeod, A., Armitage, S.J., Kabaciński, J. & Gamble, C.S. (2014) The potential of cryptotephra and OSL dating for refining the chronology of open-air archaeological windblown sand sites: a case study from Mirkowice 33, northwest Poland. *Quaternary Geochronology*, 20, 99–108.
Hunt, J.B. & Hill, P.G. (1993) Tephra geochemistry: a discussion of some persistent analytical problems. *The Holocene*, 3, 271–278.
Jensen, B.J.L., Pyne-O'Donnell, S., Plunkett, G., Froese, D.G., Hughes, P.D.M., Sigl, M. et al. (2014) Transatlantic distribution of the Alaskan White River Ash. *Geology*, 42, 875–878.
Johansson, H., Lind, E.M. & Wastegård, S. (2017) Compositions of glass in proximal tephras from eruptions in the Azores archipelago and their links with distal sites in Ireland. *Quaternary Geochronology*, 40, 120–128.
John Lowe, J. & Hoek, W.Z., INTIMATE group. (2001) Inter-regional correlation of palaeoclimatic records for the Last Glacial—Interglacial Transition: a protocol for improved precision recommended by the INTIMATE project group. *Quaternary Science Reviews*, 20, 1175–1187.
Jones, G., Davies, S.M., Staff, R.A., Loader, N.J., Davies, S.J. & Walker, M.J.C. (2019) Traces of volcanic ash from the Mediterranean, Iceland and North America in a Holocene record from south Wales, UK. *Journal of Quaternary Science*, 35, 163–174.
Jónsson, D.F., Gudmundsdóttir, E.R., Larsen, G., Óladóttir, B.A., Erlendsson, E., Eddudóttir, S.D. et al. (2020) The multi-component Hekla Ö tephra, Iceland: a complex widespread mid-Holocene tephra layer. *Journal of Quaternary Science*, 35, 410–421.
Kalliokoski, M., Wastegård, S. & Saarinen, T. (2019) Rhyolitic and dacitic component of the Askja 1875 tephra in southern and central Finland: first step towards a Finnish tephrochronology. *Journal of Quaternary Science*, 34, 29–39.
Kalliokoski, M., Guðmundsdóttir, E.R. & Wastegård, S. (2020) Hekla 1947, 1845, 1510 and 1158 tephra in Finland: challenges of tracing tephra from moderate eruptions. *Journal of Quaternary Science*, 35, 803–816.
Kalliokoski, M., Guðmundsdóttir, E.R., Wastegård, S., Jokinen, S. & Saarinen, T. (2023) A Holocene tephrochronological framework for Finland. *Quaternary Science Reviews*, 312, 108173.
Kinder, M., Wulf, S., Appelt, O., Hardiman, M., Żarczyński, M. & Tylmann, W. (2020) Late-Holocene ultra-distal cryptotephra discoveries in varved sediments of Lake Żabińskie, NE Poland. *Journal of Volcanology and Geothermal Research*, 402, 106988.
Kuno, H. (1966) Lateral variation of basalt magma type across continental margins and island arcs. *Bulletin Volcanologique*, 29, 195–222.
Lamoureux, S.F. (1994) Embedding unfrozen lake sediments for thin section preparation. *Journal of Paleolimnology*, 10, 141–146.
Lane, C.S., Brauer, A., Blockley, S.P.E. & Dulski, P. (2013) Volcanic ash reveals time-transgressive abrupt climate change during the Younger Dryas. *Geology*, 41, 1251–1254.
Lane, C.S., Cullen, V.L., White, D., Bramham-Law, C.W.F. & Smith, V.C. (2014) Cryptotephra as a dating and correlation tool in archaeology. *Journal of Archaeological Science*, 42, 42–50.
Langdon, P.G. & Barber, K.E. (2004) Snapshots in time: precise correlations of peat-based proxy climate records in Scotland using mid-Holocene tephras. *The Holocene*, 14, 21–33.
Larsen, G., Dugmore, A. & Newton, A. (1999) Geochemistry of historical-age silicic tephras in Iceland. *The Holocene*, 9, 463–471.
Larsen, G., Eiríksson, J., Knudsen, K.L. & Heinemeier, J. (2002) Correlation of late Holocene terrestrial and marine tephra markers, north Iceland: implications for reservoir age changes. *Polar Research*, 21, 283–290.
Larsen, G., Newton, A.J., Dugmore, A.J. & Vilmundardóttir, E.G. (2001) Geochemistry, dispersal, volumes and chronology of Holocene silicic tephra layers from the Katla volcanic system, Iceland. *Journal of Quaternary Science*, 16, 119–132.
Larsen, G., Róbertsdóttir, B.G., Óladóttir, B.A. & Eiríksson, J. (2020) A shift in eruption mode of Hekla volcano, Iceland, 3000 years ago: two-coloured Hekla tephra series, characteristics, dispersal and age. *Journal of Quaternary Science*, 35, 143–154.
Lincoln, P., Tjallingii, R., Kosonen, E., Ojala, A., Abrook, A.M. & Martin-Puertas, C. (2025) Disruption of boreal lake circulation in response to mid-Holocene warmth; evidence from the varved sediments of Lake Nautajärvi, southern Finland. *Science of the Total Environment*, 964, 178519.
Lind, E.M. & Wastegård, S. (2011) Tephra horizons contemporary with short early Holocene climate fluctuations: new results from the Faroe Islands. *Quaternary International*, 246, 157–167.
Lotter, A.F. & Lemcke, G. (1999) Methods for preparing and counting biochemical varves. *Boreas*, 28, 243–252.
Lunkka, J.P., Palmu, J.P. & Seppänen, A. (2020) Deglaciation dynamics of the Scandinavian Ice Sheet in the Salpausselkä zone, southern Finland. *Boreas*, 50, 404–418.
Mackay, H., Plunkett, G., Jensen, B.J.L., Aubry, T.J., Corona, C., Kim, W.M. et al. (2022) The 852/3 CE Mount Churchill eruption: examining the potential climatic and societal impacts and the timing of the Medieval Climate Anomaly in the North Atlantic region. *Climate of the Past*, 18, 1475–1508.

MacLeod, A., Brunnberg, L., Wastegård, S., Hang, T. & Matthews, I.P. (2014) Lateglacial cryptotephra detected within clay varves in Östergötland, south-east Sweden. *Journal of Quaternary Science*, 29, 605–609.

Martín-Puertas, C., Jiménez-Espejo, F., Martínez-Ruiz, F., Nieto-Moreno, V., Rodrigo, M., Mata, M.P. et al. (2010) Late Holocene climate variability in the southwestern Mediterranean region: an integrated marine and terrestrial geochemical approach. *Climate of the Past*, 6, 807–816.

Martin-Puertas, C., Walsh, A.A., Blockley, S.P.E., Harding, P., Biddulph, G.E. & Palmer, A. et al. (2021) The first Holocene varve chronology for the UK: based on the integration of varve counting, radiocarbon dating and tephrostratigraphy from Diss Mere (UK). *Quaternary Geochronology*, 61, 101134.

Meara, R.H., Thordarson, T., Pearce, N.J.G., Hayward, C. & Larsen, G. (2020) A catalogue of major and trace element data for Icelandic Holocene silicic tephra layers. *Journal of Quaternary Science*, 35, 122–142.

Müller, D.J.M., Neugebauer, I., Kearney, R.J., Schwab, M.J., Appelt, O., Czymzik, M. et al. (2025) Constraining the Baltic Sea sediment chronology using tephrochronology. *Geology*, 53, 743–747.

Ojala, A.E.K. & Tiljander, M. (2003) Testing the fidelity of sediment chronology: comparison of varve and paleomagnetic results from Holocene lake sediments from central Finland. *Quaternary Science Reviews*, 22, 1787–1803.

Ojala, A.E.K., Saarinen, T. & Salonen, V.-P. (2000) Preconditions for the formation of annually laminated lake sediments in southern and central Finland. *Boreal Environment Research*, 5, 243–255.

Óladóttir, B.A., Larsen, G. & Sigmarsson, O. (2011) Holocene volcanic activity at Grímsvötn, Bárdarbunga and Kverkfjöll subglacial centres beneath Vatnajökull, Iceland. *Bulletin of Volcanology*, 73, 1187–1208.

Óladóttir, B.A., Sigmarsson, O., Larsen, G. & Thordarson, T. (2008) Katla volcano, Iceland: magma composition, dynamics and eruption frequency as recorded by Holocene tephra layers. *Bulletin of Volcanology*, 70, 475–493.

Persson, C. (1966) Försök till tefrokronologisk datering av några svenska torvmossar. *Geologiska Föreningen i Stockholm Förhandlingar*, 88, 361–394.

Pearson, C., Sigl, M., Burke, A., Davies, S., Kurbatov, A., Severi, M. et al. (2022) Geochemical ice-core constraints on the timing and climatic impact of Aniakchak II (1628 BCE) and Thera (Minoan) volcanic eruptions. *PNAS Nexus*, 1, 1–12.

Pilcher, J.R. & Hall, V.A. (1992) Towards a tephrochronology for the Holocene of the north of Ireland. *The Holocene*, 2, 255–259.

Pilcher, J.R. & Hall, V.A. (1996) Tephrochronological studies in northern England. *The Holocene*, 6, 100–105.

Plunkett, G. & Pilcher, J.R. (2018) Defining the potential source region of volcanic ash in northwest Europe during the Mid- to Late Holocene. *Earth–Science Reviews*, 179, 20–37.

Plunkett, G., Sigl, M., McConnell, J.R., Pilcher, J.R. & Chellman, N.J. (2023) The significance of volcanic ash in Greenland ice cores during the Common Era. *Quaternary Science Reviews*, 301, 107936.

Prestvik, T. (1985) *Petrology of Quaternary volcanic rocks from Öræfi, southeast Iceland. Report 21*. Trondeim: Geologisk Institutt, Norges Tekniske Hojskole.

Pyne-O'donnell, S. (2011) The taphonomy of Last Glacial–Interglacial Transition (LGIT) distal volcanic ash in small Scottish lakes: taphonomy of LGIT distal volcanic ash in Scottish lakes. *Boreas*, 40, 131–145.

Rainio, H. (1982) Lössiä Etelä-Suomessa Toisen Salpausselän distaalipuolella. *Geologi*, 34, 134–136.

Reilly, E. & Mitchell, F.J. (2015) Establishing chronologies for woodland small hollow and mor humus deposits using tephrochronology and radiocarbon dating. *The Holocene*, 25, 241–252.

Reimer, P.J., Austin, W.E.N., Bard, E., Bayliss, A., Blackwell, P.G., Bronk Ramsey, C. et al. (2020) The IntCal20 Northern Hemisphere radiocarbon age calibration curve (0–55 cal kBP). *Radiocarbon*, 62, 725–757.

Renberg, I. & Hansson, H. (2008) The HTH sediment corer. *Journal of Paleolimnology*, 40, 655–659.

Rothwell, R.G. & Croudace, I.W. (2015) Micro-XRF studies of sediment cores: a perspective on capability and application in the environmental sciences. In: Croudace, I. & Rothwell, R. (Eds.) *Micro-XRF studies of sediment cores: applications of a non-destructive tool for the environmental sciences*. Dordrecht: Springer Netherlands, pp. 1–21.

Saarinen, T. & Wenho, H. (2005) Minijääsormi sekä muita uusia ja vanhoja ideoita järvisedimentin talvikaikaukseen. Geologian tutkijapäivät 14.-15.3.2005, Turku. *Congress Abstract Book* (in Finnish), 72–73.

Saarni, S., Lensu, A., Tammelin, M., Haltia, E. & Saarinen, T. (2017) Winter climate signal in boreal clastic-biogenic varves: a comprehensive analysis of three varved records from 1890 to 1990 AD with meteorological and hydrological data from Eastern Finland. *GFF*, 139, 314–326.

Saarni, S., Muschitiello, F., Weege, S. & Brauer, A. (2016a) A late Holocene record of solar-forced atmospheric blocking variability over Northern Europe inferred from varved lake sediments of Lake Kuninkaisenlampi. *Quaternary Science Reviews*, 154, 100–110.

Saarni, S., Saarinen, T. & Dulski, P. (2016b) Between the North Atlantic Oscillation and the Siberian High: a 4000-year snow accumulation history inferred from varved lake sediments in Finland. *The Holocene*, 26, 423–431.

Saarni, S., Saarinen, T. & Lensu, A. (2015) Organic lacustrine sediment varves as indicators of past precipitation changes: a 3,000-year climate record from Central Finland. *Journal of Paleolimnology*, 53, 401–413.

Salmi, M. (1948) The Hekla ashfalls in Finland. AD 1947. *Comptes Rendus de la Société Geologique de Finlande*, 21, 8–96.

Salminen, S., Saarni, S. & Saarinen, T. (2023) Sensitivity of varve biogenic component to climate in eastern and central Finland. *Journal of Paleolimnology*, 70, 113–130.

Salminen, S., Tammelin, M., Jilbert, T., Fukumoto, Y. & Saarni, S. (2021) Human actions were responsible for both initiation and termination of varve preservation in Lake Vesijärvi, southern Finland. *Journal of Paleolimnology*, 66, 207–227.

Sigmarsson, O., Condomines, M. & Fourcade, S. (1992) A detailed Th, Sr and O isotope study of Hekla: differentiation processes in an Icelandic volcano. *Contributions to Mineralogy and Petrology*, 112, 20–34.

Sinnl, G., Winstrup, M., Erhardt, T., Cook, E., Jensen, C.M., Svensson, A. et al. (2022) A multi-ice-core, annual-layer-counted Greenland ice-core chronology for the last 3800 years: GICC21. *Climate of the Past*, 18, 1125–1150.

Steinthorsson, S., Oskarsson, N. & Sigvaldason, G.E. (1985) Origin of alkali basalts in Iceland: a plate tectonic model. *Journal of Geophysical Research: Solid Earth*, 90, 10027–10042.

Sverrisdottir, G. (2007) Hybrid magma generation preceding Plinian silicic eruptions at Hekla, Iceland: evidence from mineralogy and chemistry of two zoned deposits. *Geological Magazine*, 144, 643–659.

Tipping, R., Ashmore, P., Davies, A.L., Haggart, B.A., Moir, A., Newton, A. et al. (2008) Prehistoric *Pinus* woodland dynamics in an upland landscape in northern Scotland: the roles of climate change and human impact. *Vegetation History and Archaeobotany*, 17, 251–267.

Turney, C.S.M. (1998) Extraction of rhyolitic component of Vedde microtephra from minerogenic lake sediments. *Journal of Paleolimnology*, 19, 199–206.

Vinther, B.M., Clausen, H.B., Johnsen, S.J., Rasmussen, S.O., Andersen, K.K., Buchardt, S.L. et al. (2006) A synchronized dating of three Greenland ice cores throughout the Holocene. *Journal of Geophysical Research: Atmospheres*, 111, D13102.

Walsh, A.A., Blockley, S.P.E., Milner, A.M. & Martin-Puertas, C. (2023) Updated age constraints on key tephra markers for NW Europe based on a high-precision varve lake chronology. *Quaternary Science Reviews*, 300, 107897.

Walsh, A.A., Blockley, S.P.E., Milner, A.M., Matthews, I.P. & Martin-Puertas, C. (2021) Complexities in European Holocene cryptotephra dispersal revealed in the annually laminated lake record of Diss Mere, East Anglia. *Quaternary Geochronology*, 66, 101213.

Wastegård, S. (2005) Late Quaternary tephrochronology of Sweden: a review. *Quaternary International*, 130, 49–62.

Wastegård, S., Johansson, H. & Pacheco, J.M. (2020) New major element analyses of proximal tephras from the Azores and suggested correlations with cryptotephras in North-West Europe. *Journal of Quaternary Science*, 35, 114–121.

Watson, E.J., Swindles, G.T., Lawson, I.T. & Savov, I.P. (2016) Do peatlands or lakes provide the most comprehensive distal tephra records? *Quaternary Science Reviews*, 139, 110–128.

Watson, E.J., Swindles, G.T., Lawson, I.T., Savov, I.P. & Wastegård, S. (2017) The presence of Holocene cryptotephra in Wales and southern England. *Journal of Quaternary Science*, 32, 493–500.

Wulf, S., Dräger, N., Ott, F., Serb, J., Appelt, O., Guðmundsdóttir, E. et al. (2016) Holocene tephrostratigraphy of varved sediment records from Lakes Tiefer See (NE Germany) and Czechowskie (N Poland). *Quaternary Science Reviews*, 132, 1–14.

Zillén, L.M., Wastegård, S. & Snowball, I.F. (2002) Calendar year ages of three mid-Holocene tephra layers identified in varved lake sediments in west central Sweden. *Quaternary Science Reviews*, 21, 1583–1591.

Żarczyński, M., Wacnik, A. & Tylmann, W. (2019) Tracing lake mixing and oxygenation regime using the Fe/Mn ratio in varved sediments: 2000 year-long record of human-induced changes from Lake Żabińskie (NE Poland). *Science of the Total Environment*, 657, 585–596.